Case Studies in Thermal Engineering 75 (2025) 107145

Contents lists available at ScienceDirect

Case Studies in Thermal Engineering

journal homepage: www.elsevier.com/locate/csite

Hybrid geometric optimization of wavy tubes with Y-shaped fins for enhanced solidification in latent heat storage systems

Attia Boudjemline [a], Khalil Hajlaoui [b,*], Hayder I. Mohammed [c], Nashmi H. Alrasheedi [b], Wahiba Yaïci [d], Mohammad Ghalambaz [e,f,**], Pouyan Talebidadehsardari [g], Nidhal Ben Khedher [h]

[a] Department of Industrial Engineering, University of Ha'il, Ha'il, Saudi Arabia
[b] College of Engineering, Imam Mohammad Ibn Saud Islamic University (IMSIU), Riyadh, Saudi Arabia
[c] Department of Cooling and Air Conditioning Engineering, Imam Ja'afar Al-Sadiq University, Baghdad, Iraq
[d] CanmetENERGY Research Centre, Natural Resources Canada, 1 Haanel Drive, Ottawa, Ontario, Canada
[e] Department of Mathematical Sciences, Saveetha School of Engineering, SIMATS, Chennai, India
[f] Refrigeration and Air Conditioning Technical Engineering Department, College of Technical Engineering, The Islamic University, Najaf, Iraq
[g] Power Electronics, Machines and Control (PEMC) Institute, University of Nottingham, Nottingham, UK
[h] Department of Mechanical Engineering, University of Ha'il, Ha'il, Saudi Arabia

GRAPHICAL ABSTRACT

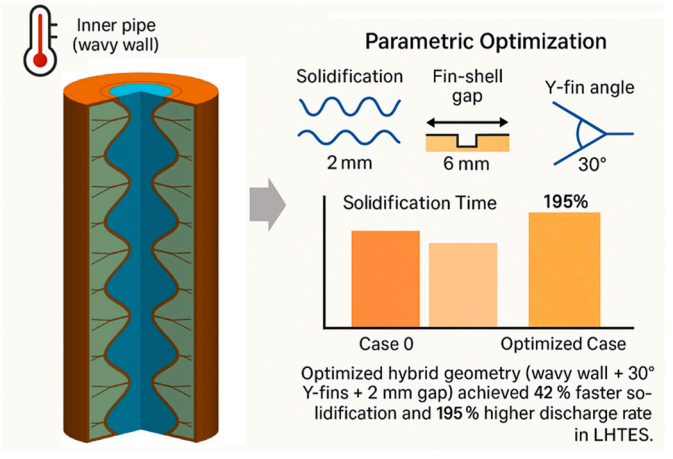

* Corresponding author.
** Corresponding author. Department of Mathematical Sciences, Saveetha School of Engineering, SIMATS, Chennai, India.
E-mail addresses: kmhajlaoui@imamu.edu.sa (K. Hajlaoui), m.ghalambaz@gmail.com (M. Ghalambaz).

https://doi.org/10.1016/j.csite.2025.107145
Received 20 June 2025; Received in revised form 6 September 2025; Accepted 26 September 2025
Available online 29 September 2025

ARTICLE INFO

Keywords:
Phase change material (PCM)
Wavy tube geometry
Y-shaped fins
Solidification enhancement
Numerical simulation

ABSTRACT

This study addresses the inherent low thermal conductivity of phase change materials (PCMs) by introducing a hybrid passive enhancement strategy that integrates wavy inner tube geometry with Y-shaped fin arrays within a vertical double-pipe heat exchanger. The novelty lies in optimizing both macro-scale surface area and micro-scale heat diffusion paths to accelerate solidification. A comprehensive parametric analysis was conducted using ANSYS Fluent with enthalpy-porosity method, examining 18 cases with varying wave amplitudes (2.5–10 mm), fin lengths, Y-fin angles (15°–30°), and fin-to-shell distances (2–6 mm). Results show that Case 17, featuring a 10 mm wave amplitude, 2 mm fin-shell gap, and 30° Y-fin angle, achieved complete solidification in 1565s (42 % faster than the smooth-wall baseline and recorded a peak discharge rate of 113.14W, nearly tripling the base case's 38.3W. These improvements are attributed to enhanced natural convection, reduced thermal resistance, and uniform heat distribution. Compared to previously reported designs, the proposed configuration offers a synergistic gain in both heat transfer rate and PCM utilization. This work is significant as it demonstrates that coupling geometric and fin-based strategies in a hybrid design can substantially overcome PCM thermal limitations, paving the way for more efficient and compact thermal energy storage systems.

1. Introduction

Declining availability of fossil fuels has led policymakers to look for renewable energy sources as a solution to limit climate change and energy supply for buildings [1]. Although these systems offer high potential, they are slowed down by constraints such as intermittent energy supply and compromised thermal efficiency [2,3]. In order to improve reliability, various energy storage technologies have been envisioned, including Latent Heat Thermal Energy Storage (LHTES), which stores thermal energy in the form of Phase Change Materials (PCMs) [4,5]. While they are superior in various aspects, PCMs have poor thermal conductivity and slow-speed thermal diffusion, which makes them ineffective in thermal management applications [5,6]. Different research studies have investigated different improvement techniques such as nanoparticle incorporation [7], the inclusion of fins [8–12], composite PCM development [13], geometry adjustments [14,15], and applying metal foams [16] to fill the gap between these challenges. Of the developed strategies, geometry adjustment and the inclusion of fins have proven to be one of the most effective means [17,18].

Jing et al. [19] combined magnetic multi-walled carbon nanotubes and copper metal foam under a magnetic field to improve the ice thermal energy storage process. Their results show that the right combination of magnetic field intensity and material configuration can lower the supercooling degree by 86.8 % and shorten the full thermal cycle by 39.8 %, while boosting storage and release rates by over 50 %. Du et al. [20] designed a 3D numerical model and validated it experimentally to investigate the effect of metal foam porosity and pore density on the phase change heat storage system. Using Taguchi methods, they found that porosity has a stronger impact than pore density on the melting-solidification process. With a porosity of 0.97 and pore density of 30 PPI, the system achieved a 67.46 % reduction in phase change time and nearly doubled the heat charging and discharging efficiency, though the total absorbed and released heat slightly decreased. Hasan et al. [21] examined the effect of loading nanoparticles in a finned tank system on the unsteady solidification process. The Galerkin-based simulations by them show that an increased shape factor (m) and volume fraction (φ) of the nanoparticles decrease the solidification time by about 6.96 % and 26.9 %, respectively. The lowest process time recorded was about 641 s, reflecting how some nanoparticle arrangements can significantly improve the thermal discharge rate. Khoshaim et al. [22] explored the influence of nanoparticle-improved conduction throughout solidification in a tank with a curved cold surface having fins. Their findings indicated that the nanoparticle insertion has extended the solidification time by 26.71 %. Their adaptive grid technique and validation provided reliable optimization methods for improving the productivity of the system. Samaii et al. [23] investigated a triplex chamber LHTES with hybrid TiO–AlO nanoparticles to investigate the impact of nanoparticle shape, thermal radiation, and volume fraction. They found that optimal solidification occurs when the volume fraction of the nanoparticle is 0.048, thermal radiation is 0.777, and the shape factor is 15.29. Alam et al. [24] carried out numerical simulations on the melting and solidification behavior of PCM in segmented composite PCM triplex-tube system. Segmentation of the system into 32 pure PCM and composite PCM segments (with copper metal foam) reduced melting time by 23 % and solidification time by 77 % compared to a single-segment model. Beyond 32 segments, further segmentation provided minimal improvement in thermal performance, and the anisotropic structure of metal foam improved the melting rates compared to random isotropic structures. Srivastava et al. [25] carried out to investigate how the use of nickel foam and MXene nanoparticles as filler material in duplex and triplex tube LHTES systems can improve solidification time. They found that this hybrid approach significantly improvs heat transfer, solidification rate, and system efficiency compared to pure PCM or nickel foam/PCM alone. The triplex tube system was superior to the duplex system by achieving a 48.40 % higher rate of solidification and improved discharge exergy, coupled with notable improvements in exergetic and overall system efficiency. Mahdi et al. [26] investigated the thermal behavior of a shell-and-tube energy storage system divided into multiple sections, each holding a PCM with a different melting point. They introduced nanoparticles into the PCMs and added cascaded metal foam to boost heat transfer within the system. Their simulation model, aligned with earlier experimental data, measured how various combinations of PCMs, nanoparticles, and metal foam influenced the system's solidification process. The best performance appeared in systems that combined multiple PCMs with cascaded foam, reducing solidification time by up to 94 %.

Adjusting the geometry of the heat exchanger has been shown to be an effective method for improving heat transfer efficiency [7,

27,28]. Elsayed et al. [29] examined the impact of aspect ratio and inner tube positioning on the solidification process within a shell-and-tube thermal energy storage system. Their numerical analysis demonstrated that shifting the inner tube position to Y = 0.2 reduced the conduction zone in the upper region, accelerating solidification. The best performance was observed with an aspect ratio of 0.5, which resulted in a reduction of 90 min in solidification time compared to the reference configuration. Kiyak et al. [30] investigated the impact of heater-cooler locations on solidification performance in a double tube heat exchanger. Their results indicated that top-cooled squares showed more rapid solidification. Srivastava et al. [31] conducted numerical simulation of eutectic PCM solidification in triplex tube heat exchangers with pentagonal, triangular, square, and circular inner tubes. Based on their findings, triangular geometries gave better performance than others and had significantly smaller solidification time and better thermal performance indices. Wang et al. [32] introduced a novel approach of tree-shaped perforated bionic fins towards enhanced solidification of phase change heat exchangers. They demonstrated that well-designed perforations strengthened natural convection, reduced discharge time, and increased PCM fill volume to the minimum extent, although greater than sufficient layers of perforations provided decreasing benefits. Aljoumaily et al. [33] analyzed the effects geometries of the inner tube on solidification in PCM in a shell and tube heat exchanger. Their findings revealed that lower flow rates lengthened solidification times, whereas spherical tubes in contact with more heat absorption than elliptical tubes. Solidification behavior was observed to initiate near the inner tube, spreading outward depending on tube shape and orientation. They also found that the circular inner tubes consistently yielded the highest thermal efficiencies under conditions tested. Abdellatif et al. [34] carried out to investigate how oval inner tubes influence solidification rate in PCM units compared to round tubes. According to their findings, vertical oval tubes caused the most significant decreases in solidification times. They reported that vertical oval tube caused nearly 19 % quicker solidification compared to circular layouts. Ameen et al. [35] quantified the role played by utilizing low-area-ratio tube arrays to augment solidification in shell and tube LHTES systems. For systems that differed in number of inner tubes, they employed numerical modeling confirmed using experimental data. The results showed that incorporating tube arrays enhanced heat transfer abilities by eliminating the natural flaw of low thermal conductivity by PCM. Kiyak et al. [36] investigated the influence of modifying double tube geometries' curvatures on the solidification process of latent thermal energy storage systems with nanoparticle-enhanced PCMs. The experiment compared a straight and curved design under various heating and cooling conditions in paraffin with copper nanoparticles in various fractions. They reported that heat transfer was significantly improved in curved geometries, which decreased solidification time by nearly half as compared to straight configurations. Zaib et al. [37] investigated the influence of duplex and triplex tube heat exchanger geometries on the solidification behavior in a LHTES system. They considered the impacts of tube material as influencing parameters on the overall solidification time. They concluded that triplex designs with precision-engineered fins reduced solidification time by over 90 %.

Regarding the top solidification enhancement techniques in LHTES systems, the use of fins in different configurations and arrangements can significantly improve heat transfer efficiency [38–41]. In this regard, Khedher et al. [42] investigated the impact of Y-shaped fins on solidification rate of the paraffin as heat storage medium encompassed in a vertical double-pipe LHTES unit. Their study demonstrated that increasing fin length decreases solidification time, with the longest fins achieving a heat release rate of 39 W, nearly 2.8 times greater than shorter fins. Guo et al. [43] investigated a novel V-shaped fin inserted in a triple-tube LHTES unit. They applied response surface methodology to identify the optimal fin structure. Their findings revealed that the use of novel fin configuration yielded at a 64.2 % reduction in solidification time and a 186.2 % increase in heat release rate compared to straight fins. Wang et al. [44] considered a set of arc-like fractal fins located in a horizontal LHTES system to see how solidification behavior changes. They found that negative curvature fins provide superior solidification efficiency and reduce the discharge time by 34.27 % compared to conventional straight fins. Du et al. [45] investigated the impact of double Y-shaped fins on solidification rate of the heat storage medium. Their numerical simulations indicated that extending fin length from 4 mm to 8 mm reduced solidification time by 38.03 %, however widening the fins lowered PCM solidification time by 7.27 %. Benaissa et al. [46] considered the curved fins in double-pipe LHTES systems and their effect on performance by changing angular curvature, base spacing, and joining angles. Their results indicated that solidification time is reduced by 22.1 % and heat recovery is enhanced by 32.0 % when the fin angular curvature is raised from 60° to 180°. Fin base spacing and joining angle optimization yields additional improvements, with the optimized curved fin geometry offering over 65 % better performance than both longitudinal fin setups and no-fin configurations in solidification rate and 190 % greater in heat recovery. Moheiseni et al. [47] numerically examine longitudinal-parabolic fins in a triplex tube LHTES system for PCM solidification enhancement. The enthalpy-porosity method is employed to analyze the influence of fin geometry, and it is established that the new parabolic fins reduce discharging time by as much as 38.5 % compared to straight fins. An extended investigation on radial and angular pitch reveals that although the radial pitch moderately influences performance, reducing the angular pitch from 120° to 60° reduces the solidification time by half, i.e., 52.3 %. In total, the most optimized design delivers a 61.8 % reduction in discharge time compared to traditional configurations. Wang et al. [48] investigate a bionic fin configuration integrated with nanoparticles, where sensitivity analysis and multi-objective optimization are used to determine optimal parameters for enhancing solidification. Through the use of NSGA-II, NSGA-III, and MOPSO optimization algorithms, the research determines that there is a significant effect of fin length and width on solidification time and heat transfer rate. The novel design improves heat transfer rates by up to 70 % and lowers solidification times by around 60 % compared to traditional fin types. Structural improvement is discovered to be more effective than nanoparticle addition, showcasing the power of fin geometry in the advancement of thermal efficiency. Guo et al. [49] applied the claw-shaped fins in a triple-tube LHTES system in order to improve the gap between melting and solidification behavior. They also analyzed the parameters including number of branches, length ratio, branch angle, and fin material, that revealed radial heat response is enhanced with longer branch length and shorter angle. Four-branch fins with the best parameters (L = 1.7, α = 21.6°) decrease phase change time by 47.8 % in comparison to V-shaped fins.

Despite numerous advancements in LHTES systems, most prior studies have focused on either modifying heat exchanger geometry or enhancing fin configurations independently, leaving a gap in understanding the combined effects of these two strategies. The

novelty of this paper lies in its hybrid approach, integrating a wavy inner tube with Y-shaped fins to synergistically enhance the heat transfer surface area and promote natural convection during solidification. The primary aim is to optimize geometric parameters (such as wave amplitude, fin angle, and fin-shell gap) to significantly reduce solidification time and increase thermal discharge rate. This work is important because it demonstrates that simultaneous macro- and micro-structural enhancements can yield up to 42 % faster solidification and 195 % higher discharge rates compared to conventional designs, offering a passive, energy-efficient solution for improving PCM-based energy storage systems in renewable and building-integrated applications.

2. Problem description

A vertical double-pipe LHTES unit using hybrid enhancement techniques of wavy pipe and Y-shaped fins is evaluated. Wavy wall is used for the inner pipe to enhance heat transfer between the HTF and PCM domain. Fins are also integrated to increase the heat transfer from the inner pipe into the PCM. Fig. 1 displays the schematic of the geometry in 3D and 2D axisymmetric models. Water passed through the inner tube to gain heat from the PCM. Due to the lack of circumferential flow inside the computational domain, the 2D axisymmetric model is used. The inner diameter of the inner and outer pipes is 36 and 80 mm, respectively. The thickness of the walls is 2 mm. The fin length is designed to ensure a 2 mm clearance between the fin tip and the inner surface of the outer pipe.

Different cases are examined to optimize the fins array and configuration of the wavy pipe to reduce the solidification time and increase the heat recovery rate compared with the cases with smooth wall (case 0) and wavy walls without fins (case 1). The thickness of the fins, fins array, Y-shaped fins stem and angle size, wave' length and amplitude of the inner pipe are all evaluated. To better understand the parameters studied, Table 1 provides the value of each parameter for different cases and Fig. 2 also displays the schematic of the main concept of various geometries assessed. In Fig. 2a–d, different fins arrays are shown while in Fig. 2e–g, the case with hybrid usage of Y-shaped fins and wavy wall, no-fin and smooth wall case and the case with only wavy wall are displayed, respectively. It should be noted that different types of the fins presented in Table 1 can be described as follows.

- **Type A:** Radial fins evenly positioned along the wave peaks and troughs of the inner tube.
- **Type B:** Radial fins positioned only at the wave peaks.
- **Type C:** Radial fins positioned only at the wave troughs.
- **Type D:** Radial fins placed at the midpoints between peaks and troughs.

The initial temperature of PCM is considered 40 °C, and the inlet temperature of the HTF is considered 10 °C. The shell is considered adiabatic to prevent heat loss to the ambience. Table 2 displays the properties of PCM. The melting point of this PCM is suitable for building applications, especially integrated with renewable energy systems such as photovoltaic/thermal systems. Although the

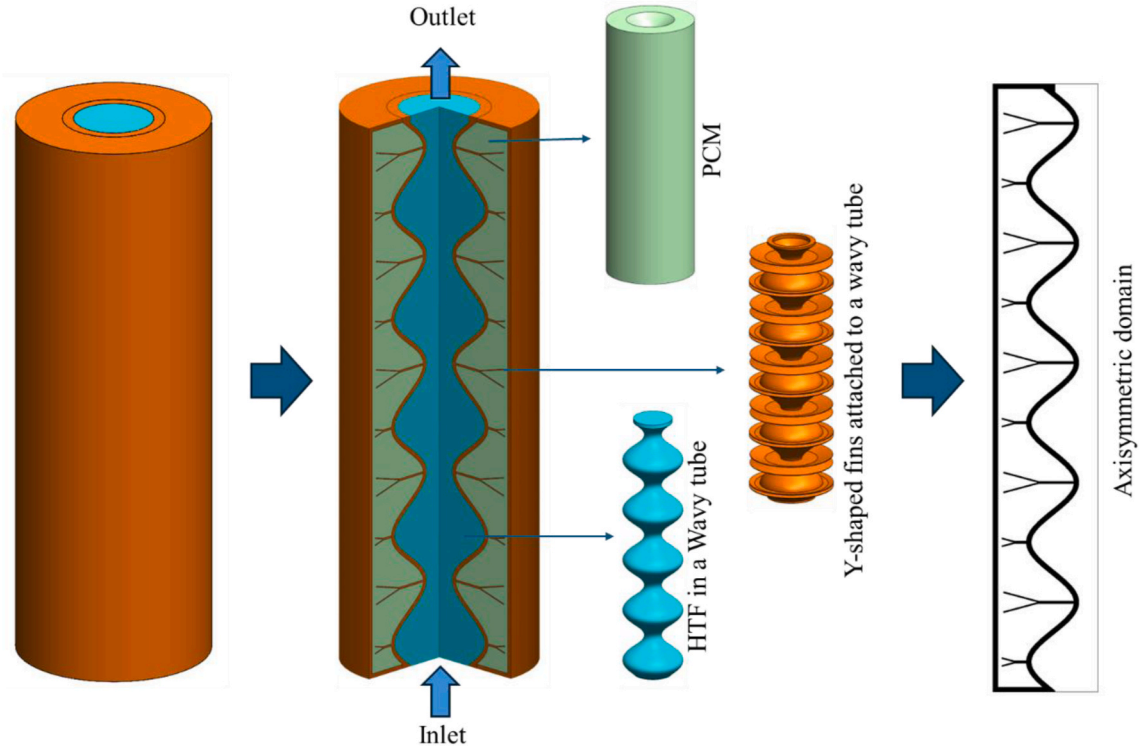

Fig. 1. Schematic of the wavy-piped heat exchanger for the containment of PCMs including the entire system and the axisymmetric domain.

Table 1
Characteristics of the geometries evaluated in this study.

	With wavy wall	With straight fins	With fins	Fins array type	Wavelength	Wave amplitude	Fin length (stem)	Y fins angle	Fin (stem) thickness	number of fins
Case 0	○	○	○	○	○	○	○	○	○	○
Case 1	●	○	○	○	25 mm	5 mm	○	○	○	○
Case 2	●	●	○	A	62.5	5	15–25	○	4.9	8
Case 3	●	●	○	A	41.67	5	15–25	○	3.2	12
Case 4	●	●	○	A	31.25	5	15–25	○	2.2	16
Case 5	●	●	○	A	25	5	15–25	○	1.77	20
Case 6	●	●	○	A	25	2.5	17.5–22.5	○	1.91	20
Case 7	●	●	○	A	25	10	10–30	○	1	20
Case 8	●	●	○	A	25	10	8–28	○	1.1	20
Case 9	●	●	○	A	25	10	6–26	○	1.23	20
Case 10	●	●	○	B	25	10	10	○	3.83	10
Case 11	●	●	○	C	25	10	30	○	1.31	10
Case 12	●	●	○	D	25	10	20	○	1.01	20
Case 13	●	○	●	A	25	10	10–30	15	1	20
Case 14	●	○	●	A	25	10	10–30	15	1	20
Case 15	●	○	●	A	25	10	10–30	15	1	20
Case 16	●	○	●	A	25	10	10–30	22.5	1	20
Case 17	●	○	●	A	25	10	10–30	30	1	20

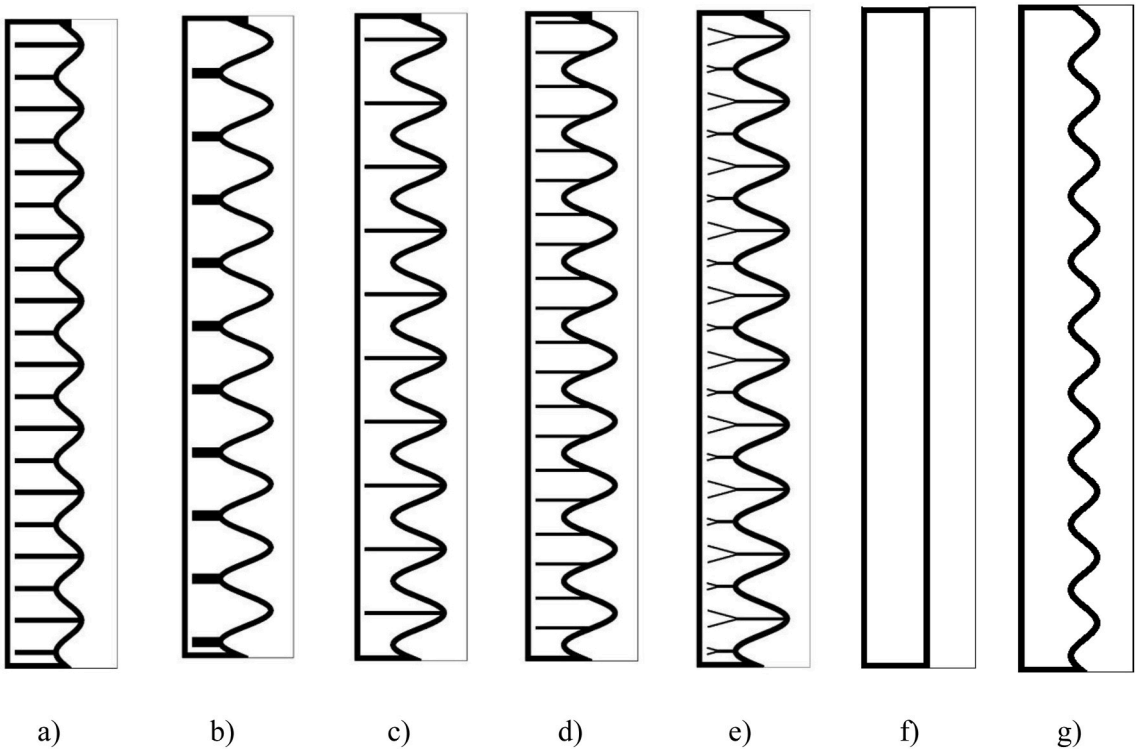

Fig. 2. Schematic of all cases evaluated in this study.

melting temperature of the PCM used in this study (34–36 °C) [50,51] is higher than the typical indoor comfort range (22–26 °C), it is well-suited for building-integrated energy systems such as solar thermal collectors, BIPV/T units, and passive façade or roof components, where surface and operating temperatures often exceed 30 °C during sunny periods. In these applications, PCM serves to store excess heat at higher temperatures for later release, aiding in peak load reduction and improving system efficiency.

It is important to note that for all simulated cases, the PCM domain volume was identical. While the geometric characteristics of the fins (shape, arrangement, length, and angle) were altered between cases, the total fin volume was kept constant. By maintaining the same fin volume, the PCM volume also remained unchanged. This approach ensures that any variations in solidification time or discharge rate are attributable purely to geometric effects rather than changes in PCM mass or capacity.

3. Mathematical modelling

The governing equations for the phase change process were formulated using the enthalpy-porosity method, based on several key assumptions. These include the application of the Boussinesq approximation to account for natural convection effects, and the use of a two-dimensional axisymmetric model to represent the computational domain. Gravity is assumed to act in the downward direction, with the heat transfer fluid (HTF) entering from the bottom of the heat exchanger. All solid boundaries are modeled with a no-slip velocity condition. The liquid PCM is considered Newtonian and incompressible, and the flow is assumed to be laminar and unsteady for both the HTF and the PCM, in accordance with the Reynolds number used in the analysis.

As a result, the governing equations can be derived from Eqs. (1)–(3) for PCM in vectorial forms [39,53]:

Table 2
The nominal thermal properties of the PCM (RT-35) [50,51].

Property	RT-35 [52]
Density (kg/m^3) (liquid)	770
Density (kg/m^3) (Solid)	880
Thermal conductivity (W/m.K)	0.2
Specific heat (J/kg K)	2000
Kinematic viscosity (m^2/s)	5×10^{-6}
Thermal expansion coefficient (K^{-1})	0.00091
Latent heat of fusion (J/kg)	160000
Melting temperature (°C)	34–36

$$\nabla.\rho\vec{V}=0 \tag{1}$$

$$\rho\frac{\partial\vec{V}}{\partial t}+\rho\left(\vec{V}.\nabla\right)\vec{V}=-\nabla P+\mu\left(\nabla^2\vec{V}\right)-\rho\beta\left(T-T_{ref}\right)\vec{g}-A_m\frac{(1-\lambda)^2}{\lambda^3+0.001}\vec{V} \tag{2}$$

$$\frac{\rho C_p\partial T}{\partial t}+\rho C_p\nabla\left(\vec{V}T\right)=k\nabla(\nabla T)-\frac{\rho L_f\partial\lambda}{\partial t}+\rho L_f\nabla\left(\vec{V}\lambda\right) \tag{3}$$

The mushy zone constant is 10^5 based on the literature [54,55]. The melt fraction is obtained based on the temperature of PCM by Eq. (4), and Eq. obtains the energy storage rate during melting (5) [56,57]:

$$\lambda=\frac{\Delta H}{L_f}=\begin{Bmatrix}0\ if\ T<T_S\\1\ if\ T>T_L\\\dfrac{T-T_S}{T_L-T_S}\ if\ T_S<T<T_L\end{Bmatrix} \tag{4}$$

$$\dot{E}_{mean}=\frac{E_{end}-E_{ini}}{t_m} \tag{5}$$

E is the total energy of the PCM, which is the summation of sensible heat and latent heat reported from the simulation software.

For the fluid flow inside the inner tube, the governing equations can be derived from Eqs. (6)–(8) based on the above-mentioned conditions:

$$\nabla\cdot V=0 \tag{6}$$

$$\rho\left(\frac{\partial V}{\partial t}+V\cdot\nabla V\right)=-\nabla P+\rho\vec{g}+\mu\nabla^2V \tag{7}$$

$$\rho C_p\left(\frac{\partial T}{\partial t}+V\cdot\nabla T\right)=k\nabla^2T \tag{8}$$

4. Numerical modelling and validation

The computational model is developed to predict the phase change behavior within the proposed system by employing a numerical framework. For this purpose, the simulation employs ANSYS Fluent solver, utilizing the well-established Semi-Implicit Method for Pressure-Linked Equations (SIMPLE) algorithm to handle the coupling between pressure and velocity fields effectively. The discretization of the governing momentum and energy equations is carried out using the Quadratic Upstream Interpolation for Convective Kinematics (QUICK) scheme. This higher-order differencing method enhances accuracy, especially for complex flow patterns typical of melting processes. For the pressure field correction, the Pressure Staggering Option (PRESTO) scheme is employed. Residuals for all governing equations -including continuity, momentum, and energy-are required to fall below a stringent threshold of 10^{-6}.

To reach the mesh independently from the size of the grid and time step, Figs. 3a and 2b present the simulation data for this purpose using case 5, which is related to the heat exchanger with wavy wall and straight fins, for the grid size analysis. Four different grids were examined, considering the cell numbers of 100k, 150k, 200kand 300k. The variation of liquid fraction as the main criterion is evaluated in Fig. 3a for different grid sizes for the time step size of 0.05s. As shown, the results are almost identical. Due to having a higher

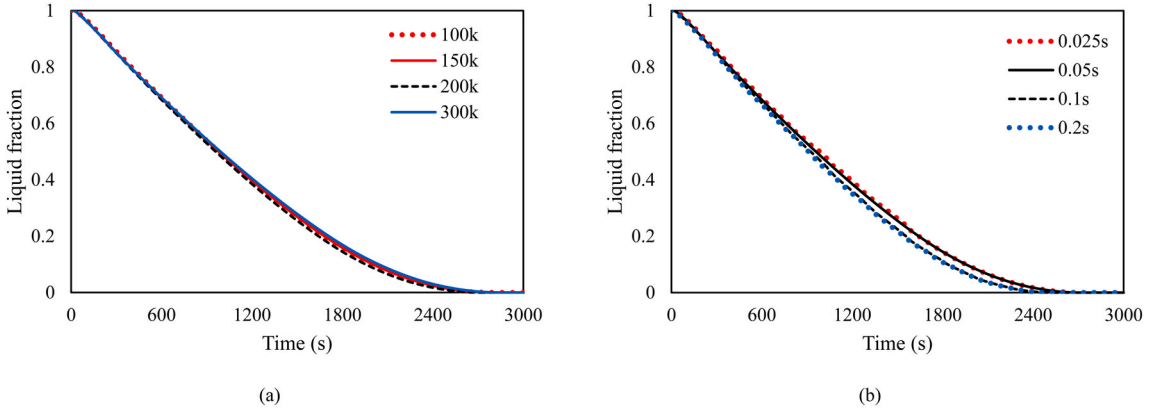

Fig. 3. Impact of a) grid number and b) time step size on the charging period.

accuracy, the mesh size of 200k was selected in this phase. The time step independence analysis was carried out using values of 0.2 s, 0.1 s, 0.05 s, and, for selected cases, an additional finer step of 0.025 s (Fig. 3b). As expected, decreasing the time step improved temporal resolution, with the smallest step (0.025 s) serving as the reference for accuracy verification. The comparison between 0.025 s and 0.05 s showed negligible differences, with a maximum deviation of less than 1.5 %, in liquid fraction during solidification, confirming that a timestep of 0.05 s is sufficiently fine for accurate results. Such small error is acceptable for most engineering applications and graphical representation of the results. Consequently, 0.05 s was selected for the main simulations as a practical compromise between accuracy and computational efficiency, following verification of negligible deviations in results when compared to finer time steps.

To validate the numerical model, the experimental data from Al-Abidi et al. [58] is used for comparison with the re-generated geometry in the present study. Al-Abidi et al. studied triplex tube heat storage unit equipped with fins. As illustrated in Fig. 4, the mean temperature of PCM during solidification simulated in this study and the study of Al-Abidi et al. align closely with each other. Quantitatively, the maximum deviation between simulated and measured temperatures is less than 1.5 °C throughout the solidification processes. Therefore, the close agreement between the quantitative temperature measurements and the numerical predictions confirms that the current numerical model is capable of accurately simulating the expected heat transfer and solidification behavior of PCMs in horizontal fined heat storage systems.

5. Results and discussion

5.1. Effect of the wavelength

Fig. 5 illustrates the fluid fracture lines of a PCM solidifying over time over six distinct geometric configurations, designated as instances 0 to 5. These scenarios illustrate the progression of the solid-liquid interface at four distinct time intervals (600 s, 1200 s, 1800 s, and 2700 s), enabling a comparative evaluation of the influence of wavy wall geometry on thermal performance. Case 0 denotes the baseline situation including vertical straight walls, exemplifying a traditional three-tube design. The solidification process is comparatively sluggish and adheres to a symmetric front, signifying minimal improvement in heat transmission due to the absence of geometric disturbances along the wall. At the conclusion of the simulation period (2700 s), a substantial fraction of the PCM persists in the liquid state, hence validating the thermal constraints of the straight-wall design.

Conversely, examples 1 to 5 include more intricate wavy wall geometries that substantially modify the solidification behavior. Case 1, characterized by a mild wave pattern, exhibits early indications of accelerated solidification relative to the baseline. The enhancement is more evident in Cases 2 to 5, when the frequency and amplitude of the wall ripples intensify. These geometric alterations increase the effective surface area for heat transmission and create localized temperature fluctuations, hence enhancing convection currents inside the PCM. As a result, heat extraction is augmented, and the phase change front progresses more swiftly. In Case 5, liquid fracture is nearly absent by 1800 s, signifying a very effective thermal design. This suggests that the integration of high-frequency, large-amplitude ripple surfaces may serve as an effective passive approach to enhance the heat extraction rate and decrease the total solidification duration in LHTES systems. Consequently, the geometric optimization of heat transfer surfaces is essential for enhancing the maximal thermal responsiveness of PCM coatings, particularly in situations necessitating quick charge/discharge cycles or elevated system density.

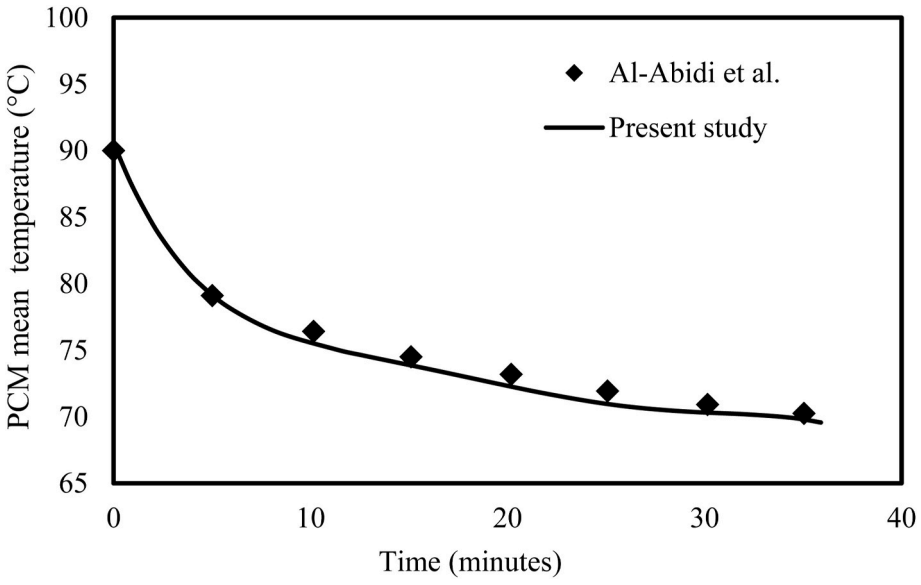

Fig. 4. Model validation during solidification using the experimental findings of Al-Abidi et al. [58].

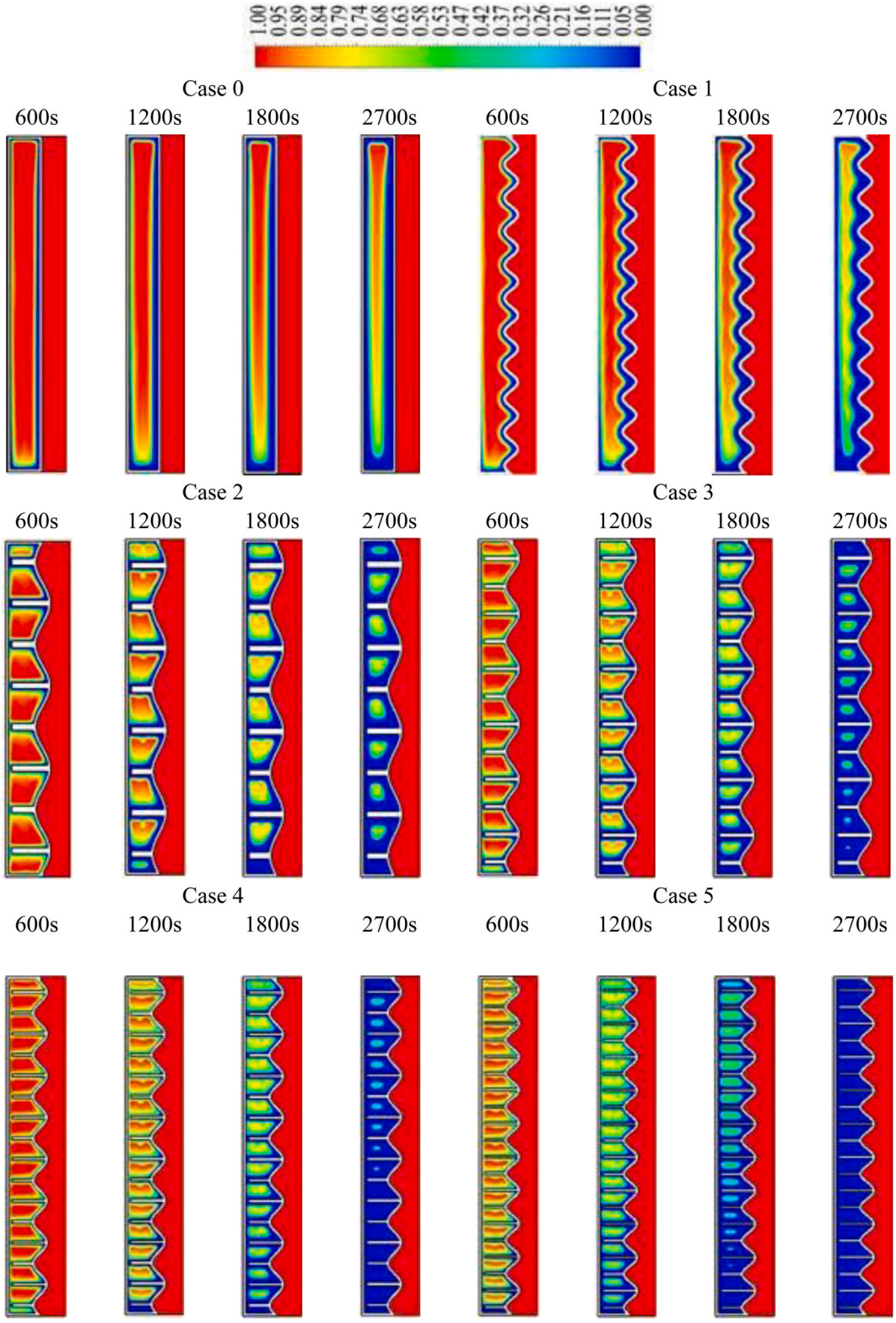

Fig. 5. Liquid fraction contours of PCM solidification at different time intervals for various cases, illustrating the impact of varying wavy wall wavelengths on thermal performance.

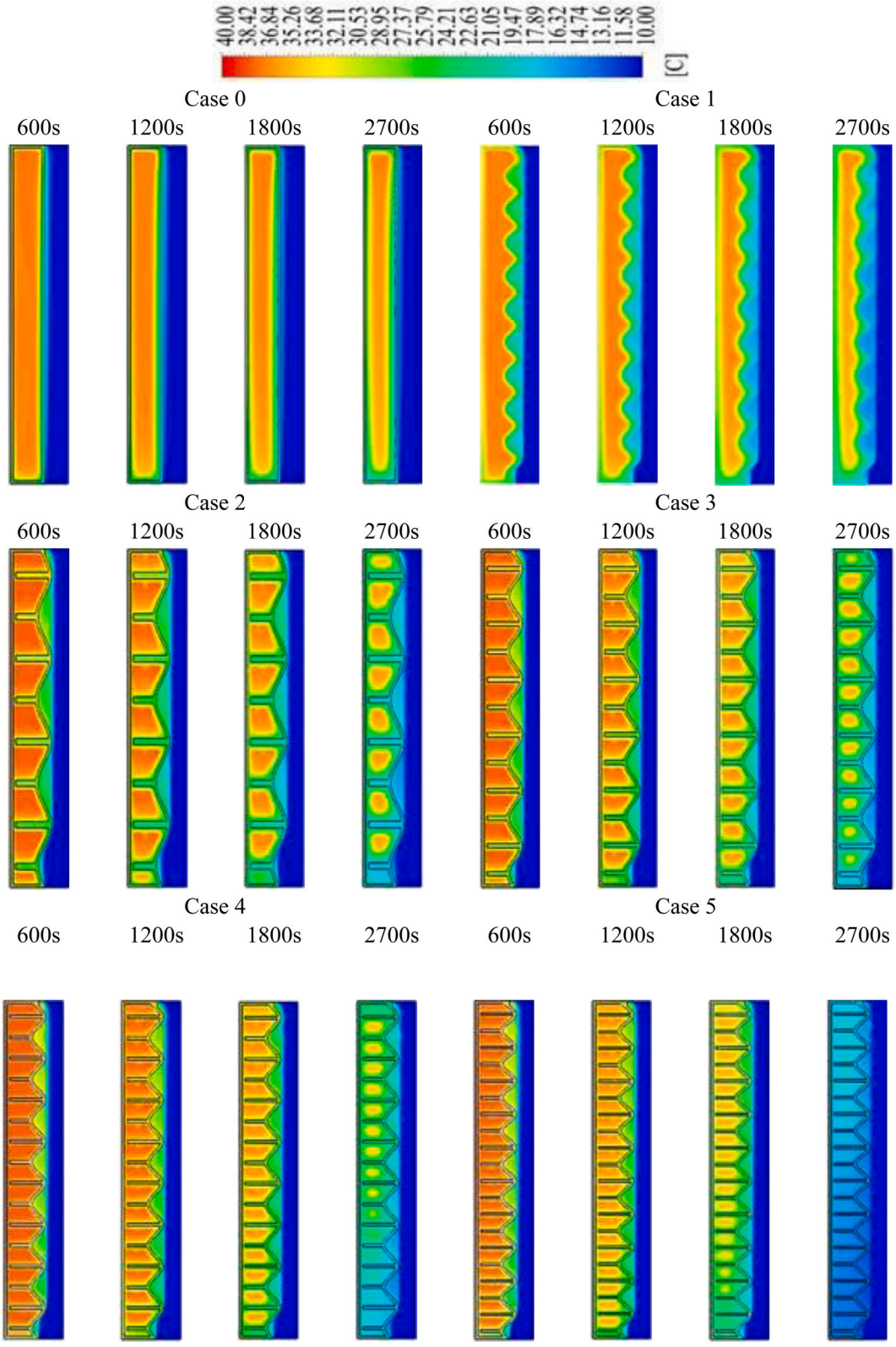

Fig. 6. Temperature contours of PCM solidification at different time intervals for various cases, illustrating the impact of varying wavy wall wavelengths on thermal performance.

Fig. 6 depicts the temperature progression in a PCM throughout the solidification process under six geometric circumstances (Cases 0–5) at time intervals of 600 s, 1200 s, 1800 s, and 2700 s. The temperature profiles offer essential insights into the thermal gradients and heat transfer efficiency of each setup. In the reference arrangement, Case 0, characterized by flat, straight walls, the temperature distribution is predominantly stratified and uniform. A sustained high-temperature zone is noted in the core area even at 2700 s, signifying sluggish conductive heat transport and a diminished thermal response attributable to the absence of convection enhancement. Conduction predominantly regulates heat transport, leading to diminished solidification rates and considerable thermal

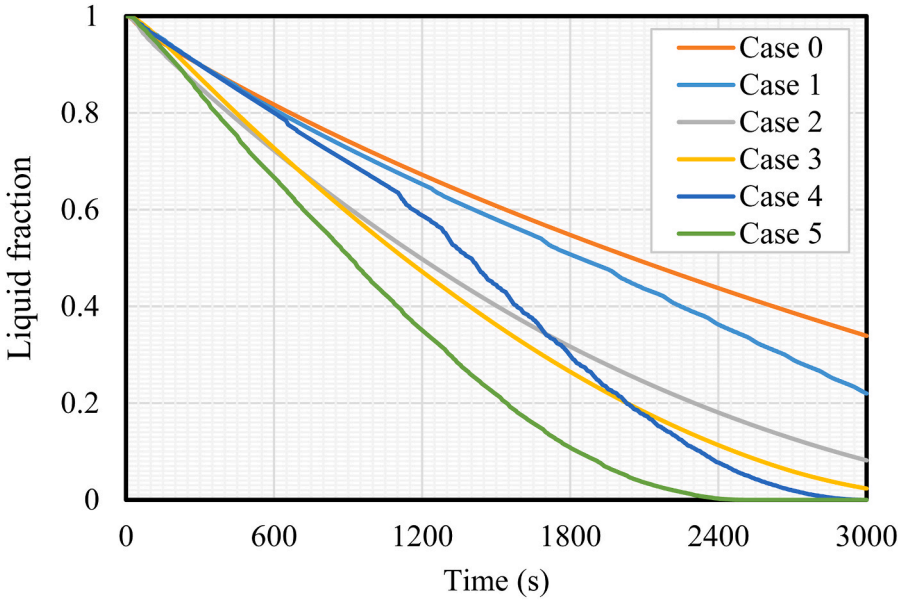

a

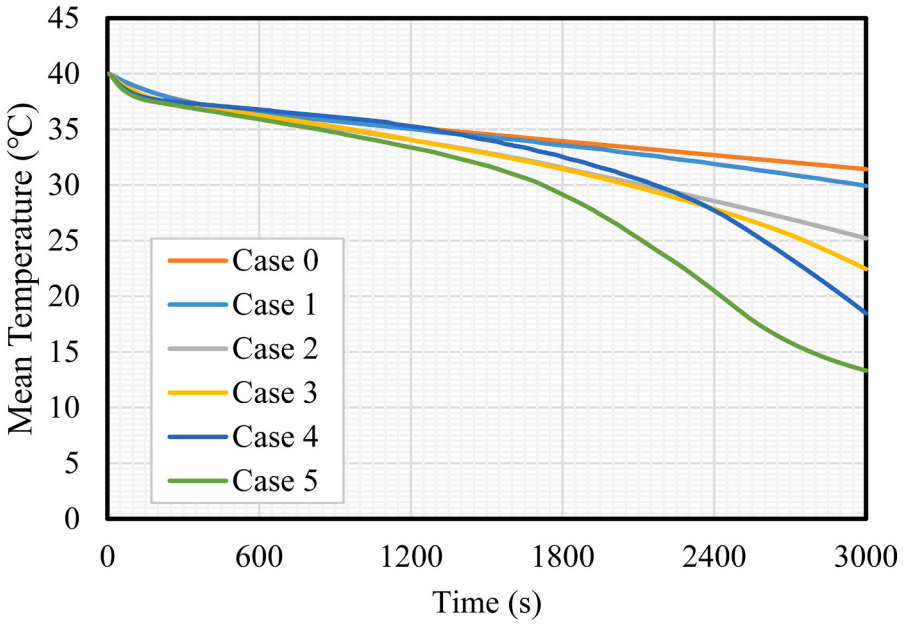

b

Fig. 7. Comparison of a) solidification times and b) mean temperature across various cases, showing the impact of wavy wall geometry on phase change completion rates.

entropy within the system.

Conversely, Cases 1–5, characterized by more intricate wavy wall geometries, have significantly distinct thermal behaviours. Insertion of surface undulations creates irregular thermal gradients and improves the localised increase of convective heat transport inside PCM. In Case 1, modest undulation generates asymmetric temperature gradients, but in Cases 2 and 3, more pronounced geometric characteristics provide numerous convection currents and an expanded contact surface area with the heat source, hence enhancing thermal diffusion into the core of the PCM. This pattern is more evident in Cases 4 and 5, where the temperature contours display fast cooling and low-temperature areas, particularly around 1800 s. In Case 5, the temperature field approaches uniformity and nears the solidification point by 2700 s, indicating enhanced thermal efficiency. The results demonstrate that undulating geometries can interfere with thermal boundary layers and enhance energy extraction from the PCM, therefore reducing solidification time. Consequently, the intentional alteration of wall geometry serves as an effective passive optimization method to enhance the thermal reactivity and dependability of latent thermal energy storage (LHTES) systems, particularly in high-performance or space-limited applications.

The upper graph in Fig. 7a illustrates the temporal development of the liquid fraction for six geometric configurations (cases 0–5), emphasizing the influence of wavy wall designs on the solidification dynamics of the PCM. Case 0, characterized by a smooth wall design, demonstrates the most gradual solidification rate, sustaining a high liquid percentage for an extended duration. Conversely, instances 1–5 (characterized by escalating wall complexity and waviness) exhibit more rapid reductions in liquid percentage, with case 5 attaining the swiftest solidification. This outcome indicates that the increased surface area and generated thermal fluctuations due to the wavy wall configuration facilitate more effective heat extraction and latent heat discharge, therefore expediting the solidification process. The most significant enhancement is shown in example 5, where the liquid percentage approaches zero by 2400 s, signifying ideal thermal efficiency resulting from convective and superconductive thermal interactions.

Fig. 7b illustrates the equivalent fluctuation in the average PCM temperature over time, offering additional insights into the efficacy of thermal management in the same scenarios. A progressive decline in temperature is noted across all instances; however, the rate and extent of this decline differ markedly. Once more, Case 0 has a greater average temperature during the process, signifying a reduced rate of thermal energy dissipation. Conversely, Cases 4 and 5 demonstrate a more pronounced and uniform reduction in temperature, indicative of their enhanced solidification properties. Case 5 demonstrates the lowest ultimate temperature among all examples, indicating its superior heat dissipation capability and expedited attainment of thermal equilibrium. This substantiates the idea that enhanced wall waviness promotes more efficient heat transport, hence facilitating the quick cooling of the PCM and phase changeover.

Fig. 7a and b collectively establish a robust association between wall geometry and phase change performance. The accelerated reduction in both liquid percentage and average temperature in instances with increased surface waviness (specifically instances 4 and 5) illustrates that optimized wavy wall configurations markedly improve heat transmission inside the PCM envelopes. The increased solidification rates noted in the fluid fraction measurements are corroborated by the swift decline in mean temperature, signifying effective latent heat removal. Conversely, State 0 continually demonstrates the least effective performance across both metrics, highlighting the shortcomings of flat-wall designs. Consequently, integrating intricate wavy wall geometries into phase-change material-based thermal energy storage systems presents a promising passive approach to expedite phase transitions and enhance thermal efficiency, especially for applications necessitating compact volume and rapid thermal response.

Table 3 displays the discharge rate (in watts) of the PCM for six geometric configurations at 2515 s, the moment when Case 5 attains complete solidification. This table quantifies the thermal energy released during solidification, so serving as a direct measure of each design's efficiency in promoting heat extraction from the PCM. Case 0, the reference scenario with flat walls, demonstrates the lowest discharge rate of 38.31 W, indicative of its restricted surface area and convection-limited enhancement, leading to diminished heat transfer efficiency. Conversely, Case 5, characterized by a more intricate wavy wall geometry, attains the greatest discharge rate of 71.87 W, indicative of complete solidification of the PCM at this juncture. This result signifies an 87.6 % enhancement compared to Case 0, validating the efficacy of geometric optimization in augmenting thermal performance.

The middle examples demonstrate progressive enhancement as wall waviness increases. Case 1 (43.51 W) presents a 13.6 % enhancement relative to Case 0, but Cases 2 (56.16 W) and 3 (60.69 W) realize advancements of 46.6 % and 58.5 %, respectively. Case 4, at 63.55 W, demonstrates a 65.9 % enhancement relative to the baseline. This trend demonstrates that augmenting the amplitude and frequency of the wavy walls markedly improves the discharge rate, chiefly owing to the enlarged surface area and the facilitation of intricate heat flow patterns that expedite phase change. The notable increase in performance from Cases 2 to 3, and subsequently from Cases 4 to 5, suggests a nonlinear correlation between wall complexity and discharge performance, potentially attributable to the synergistic interactions of surface geometry and thermal mixing inside the PCM. Case 5 surpasses all other cases in discharge rate and total phase change completion, establishing it as the most thermally efficient arrangement under the examined conditions.

Table 3
Discharge rate of the PCM for different cases at 2515 s.

Cases	Discharge rate (W)
Case 0	38.30
Case 1	43.50
Case 2	56.16
Case 3	60.69
Case 4	63.55
Case 5	71.87 (Totally solidified)

5.2. Effect of wave amplitude

This part shows the impact of wave amplitude on the solidification behavior of PCM by comparing Cases 6 (2.5 mm amplitude) and 7 (10 mm amplitude). Fig. 8, depicting the liquid fraction over time, reveals that the larger amplitude in Case 7 significantly accelerates the solidification process. This is evident from the faster reduction in liquid fraction, indicating enhanced heat transfer due to increased surface area and improved convective currents caused by the more pronounced wavy geometry. In contrast, Case 6, with its smaller amplitude, shows a slower decline in liquid fraction, aligning with the trend observed in earlier cases where less aggressive geometric modifications resulted in subdued thermal performance. These findings underscore the importance of amplitude as a critical design parameter for optimizing PCM-based thermal storage systems.

Fig. 9, which displays the temperature distribution, further supports these observations. Case 7 exhibits more uniform and rapid cooling, with lower-temperature regions developing earlier compared to Case 6. This suggests that larger amplitudes disrupt thermal boundary layers more effectively, promoting efficient heat extraction. The temperature contours in Case 7 also show fewer high-temperature zones, indicating minimized thermal resistance. Together, these figures demonstrate that increasing wave amplitude enhances both the speed and uniformity of PCM solidification, making it a viable strategy for applications requiring rapid thermal cycling. However, the trade-offs, such as potential manufacturing complexity or mechanical stress, should be considered in practical implementations. Figs. 8 and 9 are well-structured and effectively communicate the advantages of larger wave amplitudes. However, including quantitative metrics (such as exact time savings or percentage improvements in discharge rates) would strengthen the analysis. Additionally, side-by-side visual comparisons of the contours at identical time intervals could further clarify the differences between the two cases.

Fig. 10 compares the influence of wavy wall amplitudes on PCM phase change behavior by analyzing liquid fraction (a) and mean temperature (b) across Cases 5–7, with Case 5 as the baseline. The liquid fraction plot reveals that Case 7, with its 10 mm amplitude, completes solidification much faster than Cases 5 and 6. This accelerated phase transition occurs because larger wave amplitudes increase the effective heat transfer surface area and disrupt thermal boundary layers more effectively, thereby enhancing convective heat transfer and latent heat release. Case 6, featuring a 2.5 mm amplitude, shows intermediate performance, confirming that even modest increases in amplitude improve thermal response compared to the baseline straight-wall configuration.

The mean temperature plot further validates these observations, demonstrating that Case 7 achieves the most rapid and uniform cooling. The pronounced waviness in Case 7 not only boosts heat extraction efficiency but also promotes better thermal distribution, minimizing localized hot spots. In contrast, Case 5, with its straight walls, relies primarily on conduction, resulting in slower temperature reduction and prolonged thermal gradients. These results underscore how wave amplitude directly impacts PCM performance by modifying heat transfer mechanisms. The superior performance of Case 7 stems from its ability to maximize convective effects through geometric optimization, though practical implementation must balance these thermal advantages with structural and manufacturing considerations. While the figure clearly demonstrates the relationship between amplitude and thermal performance, incorporating quantitative metrics such as exact time savings or heat flux densities would provide more actionable insights. Additionally, including uncertainty ranges or statistical validation would strengthen the robustness of the conclusions. The trends align well with established heat transfer principles, but further investigation into the trade-offs between amplitude size and system durability would enhance the practical relevance of these findings.

Table 4 reveals important insights about how wavy wall amplitude affects PCM discharge performance. Case 5 (5 mm amplitude) serves as a critical reference point, demonstrating that moderate wave amplitude provides balanced performance with a discharge rate of 71.9W and complete discharge in 2515 s. The data shows a non-linear relationship between amplitude and performance - while increasing to 10 mm (Case 7) boosts discharge rate by 51 %–108.8W and cuts discharge time by 35 %, reducing to 2.5 mm (Case 6)

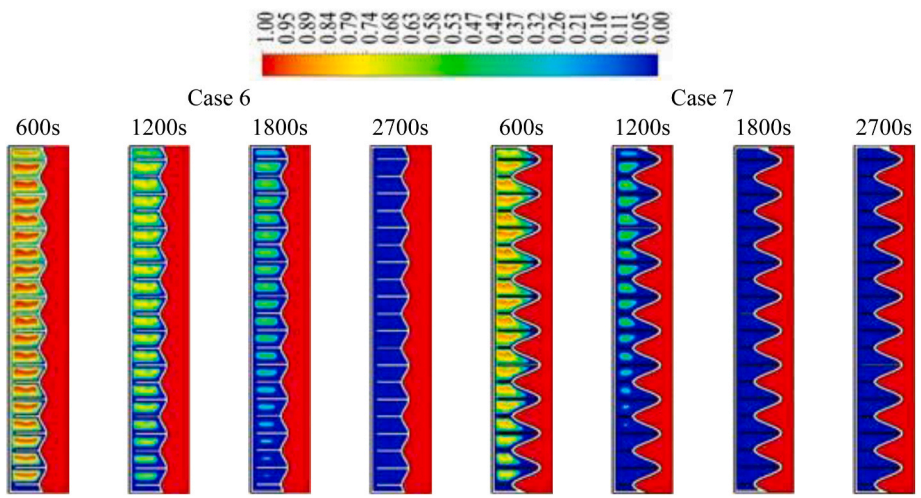

Fig. 8. Time-evolution of liquid fraction for Cases 6 (2.5 mm amplitude) and 7 (10 mm amplitude) at different time steps.

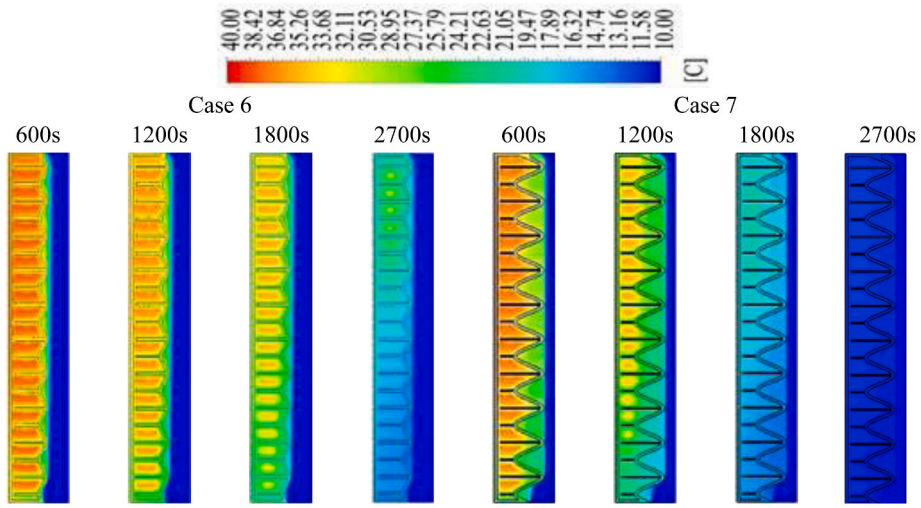

Fig. 9. Time-evolution of temperature distribution for Cases 6 (2.5 mm amplitude) and 7 (10 mm amplitude) at different time steps.

actually worsens performance compared to Case 5. This occurs because the 5 mm amplitude in Case 5 creates sufficient surface area enhancement and thermal boundary disruption to significantly improve upon straight-wall designs, while avoiding the diminishing returns that come with excessive wave complexity.

The superior performance of Case 7 (10 mm) stems from its ability to maximize both convective heat transfer and effective surface area. The deeper waves create stronger secondary flows that enhance mixing while providing more contact area between PCM and heat transfer surfaces. However, Case 6's poorer results (66.8W, 2715s) compared to Case 5 suggest there's a minimum threshold amplitude needed to overcome the natural thermal resistance of PCMs. The 5 mm amplitude in Case 5 appears to be near this threshold, providing enough geometric disturbance to improve performance without the manufacturing challenges of more extreme amplitudes. These findings highlight that amplitude optimization requires balancing thermal gains against practical constraints, with 5 mm representing a practical compromise between performance and feasibility for many applications.

5.3. Effect of the distance between the fins and shell

Fig. 11 compares the solidification behavior of PCM in Cases 8 (4 mm fin-shell gap) and 9 (6 mm gap) through liquid fraction and temperature contours at 600–2700s. The results demonstrate that smaller gaps (Case 8) significantly enhance heat transfer, evidenced by faster solidification fronts and more uniform temperature distribution compared to Case 9. This occurs because reduced fin-shell distances improve thermal contact, minimizing air gaps that act as insulating barriers. The closer proximity allows fins to more effectively conduct heat from the shell into the PCM, accelerating phase change. In contrast, Case 9's larger gap creates thermal resistance, leading to slower heat penetration and persistent liquid pockets even at 2700s. The temperature contours further validate this, showing Case 8 achieves lower core temperatures earlier due to efficient heat diffusion.

Fig. 11 effectively highlights the critical role of fin-shell contact in PCM systems. The superior performance of Case 8 aligns with heat transfer principles: conductive pathways dominate in such configurations, and smaller gaps reduce thermal resistance. However, the figure could be strengthened by including Case 7 (2 mm gap) for a complete trend analysis. The observed behaviors are justified by Fourier's Law (heat flux increases with proximity to the heat source) and the elimination of convective "dead zones" in narrow gaps. Practical applications must balance this benefit against mechanical tolerance; excessively small gaps may complicate manufacturing or induce stress during thermal cycling. Including quantitative metrics like discharge rates would further solidify the conclusions.

Fig. 12 compares the liquid fraction reduction (a) and mean temperature evolution (b) across Cases 7–9, evaluating how varying fin-shell distances (2 mm, 4 mm, and 6 mm) impact PCM solidification. The liquid fraction plot reveals that Case 7 (2 mm gap) achieves complete solidification fastest, followed by Case 8 (4 mm), while Case 9 (6 mm) lags significantly. This trend occurs because smaller gaps minimize thermal resistance between the fins and PCM, enabling more efficient conductive heat transfer. The temperature plot (b) corroborates this, showing Case 7 maintains the steepest cooling curve, as the tight fin-shell coupling ensures rapid heat extraction. In contrast, Case 9's larger gap creates a thermal bottleneck, resulting in slower temperature drops and incomplete phase change even at later stages. The intermediate performance of Case 8 demonstrates that while reduced gaps enhance heat transfer, the benefits diminish as the distance increases.

Fig. 12 effectively demonstrates the inverse relationship between fin-shell distance and thermal performance, grounded in fundamental heat transfer principles. The superior behavior of Case 7 is justified by Fourier's Law: heat conduction scales inversely with distance, making smaller gaps ideal for maximizing energy transfer. However, the figure could be improved by including error bars or statistical validation to account for experimental variability. The practical implications are clear (designers should minimize fin-shell gaps where possible) but must also consider trade-offs like mechanical stress during thermal expansion or manufacturing

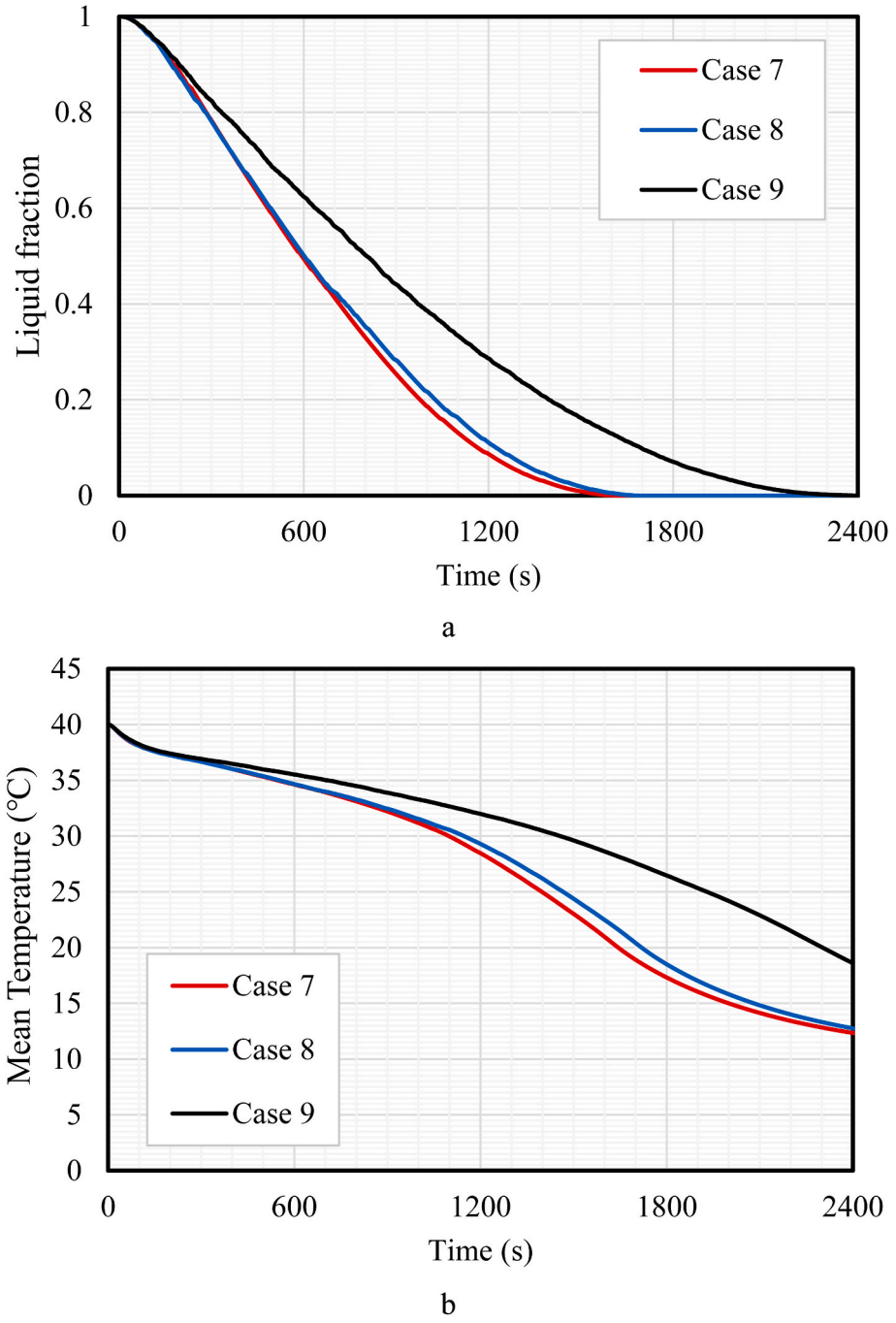

Fig. 10. Comparison of a) liquid fraction and b) mean temperature for cases 5–7 evaluating the impact of wavy wall amplitudes on PCM phase change behaviour, with Case 5 operating as the baseline configuration.

Table 4
Discharging time and rate of the PCM for different cases.

Cases	Total discharging time (s)	Discharge rate (W)
Case 5	2515	71.9
Case 6	2715	66.8
Case 7	1633	108.8

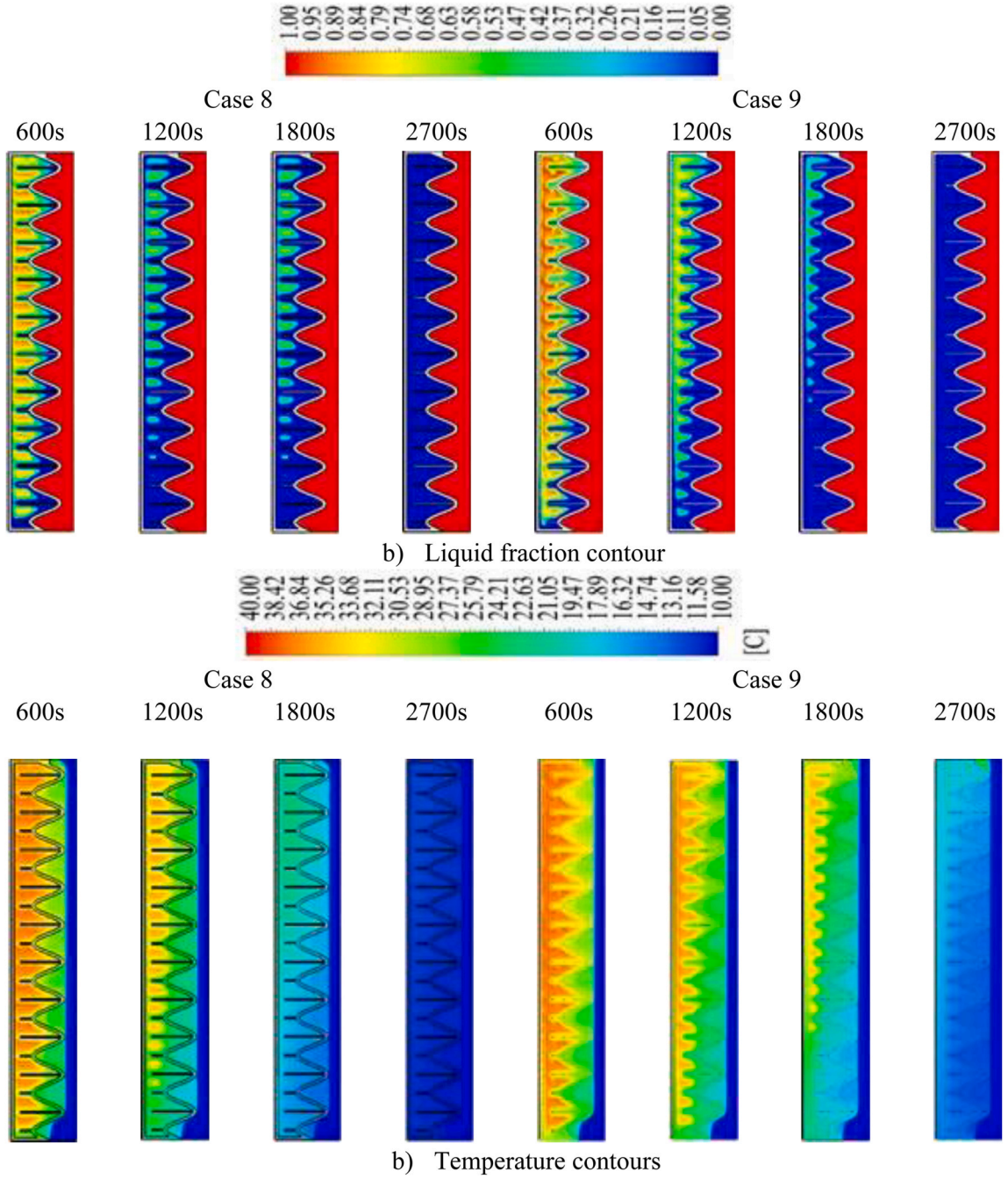

Fig. 11. Time-evolution of (a) liquid fraction and (b) temperature contours for Cases 8 and 9 at various time steps, at different distances between the fins and shell.

constraints. The absence of extreme cases (e.g., 1 mm or 8 mm gaps) limits the identification of an optimal threshold, suggesting room for further investigation. Including discharge rate data (as in Table 4) would strengthen the correlation between geometric design and thermal efficiency.

Fig. 13 compares the discharge rates of Cases 7–9, demonstrating how fin-shell distance impacts thermal performance. Case 7 (2 mm gap) achieves the highest discharge rate (108.8 W), outperforming Case 8 (4 mm) by 63 % and Case 9 (6 mm) by 163 %. This dramatic difference occurs because smaller gaps minimize thermal resistance, enabling more efficient heat conduction from fins to PCM. The 2 mm gap in Case 7 ensures optimal thermal coupling, while the larger gaps in Cases 8 and 9 introduce insulating air layers that hinder heat transfer. The results align with Fourier's Law, where heat flux declines proportionally with increased distance.

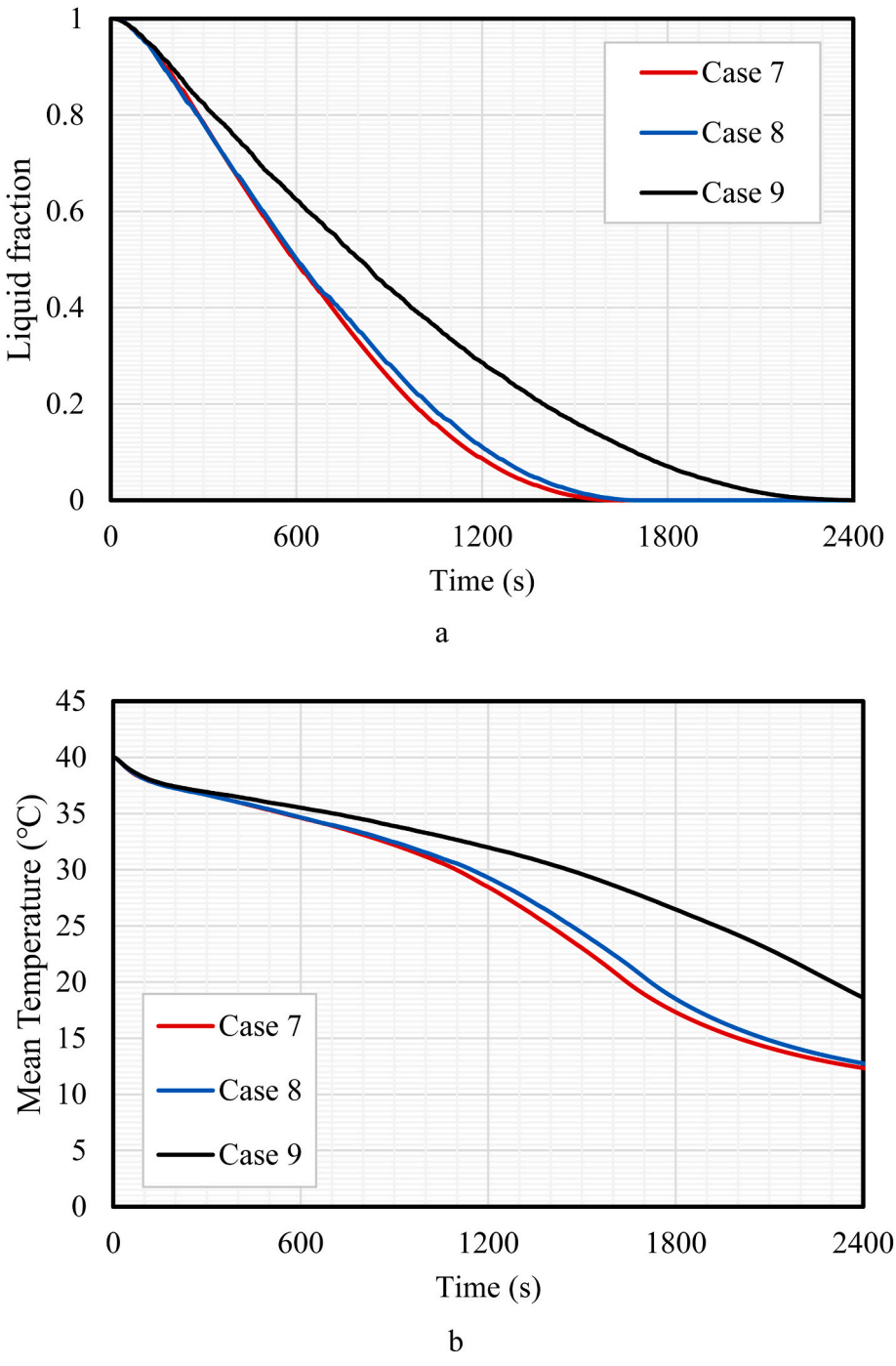

Fig. 12. Comparison of a) liquid fraction and b) mean temperature for cases 7–9 evaluating the impact of the distance between the fins and shell on PCM phase change behaviour.

5.4. Effect of fins arrangement

Fig. 14 compares three fin configurations - lower-peak (Case 10), upper-peak (Case 11), and mid-point (Case 12) attachments - through liquid fraction (a) and temperature contours (b) during solidification. The results reveal that mid-point fins (Case 12) demonstrate the most balanced performance, with faster and more uniform phase change compared to the other configurations. This occurs because mid-point attachment optimizes heat distribution by positioning fins at the thermal center of the PCM volume, enabling efficient bidirectional heat transfer both upwards and downwards. In contrast, lower-peak fins (Case 10) show slightly slower

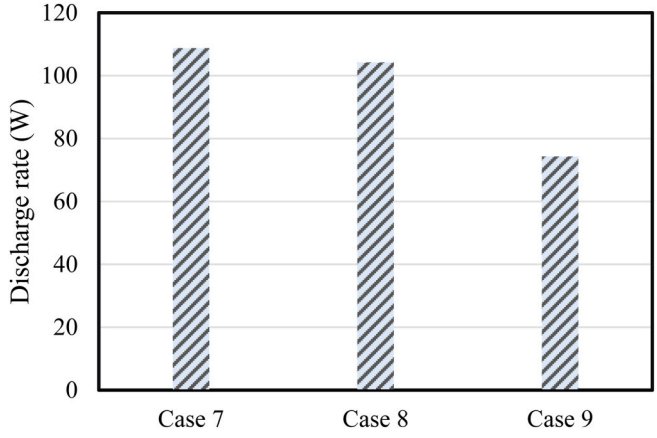

Fig. 13. Comparison of discharge rate for fin configurations (Cases 7–9).

performance due to reduced heat penetration in upper regions, while upper-peak fins (Case 11) create thermal stratification with warmer zones accumulating at the bottom. The temperature contours clearly show Case 12 achieves the most isothermal conditions, indicating superior thermal equilibration.

The superior performance of mid-point fins in Fig. 14 can be explained by fundamental heat transfer principles. By centering the fins, Case 12 minimizes the maximum thermal diffusion distance to any point in the PCM, whereas asymmetric placements in Cases 10–11 create longer heat paths to certain regions. The figure effectively demonstrates this through clear visual comparisons, though quantitative metrics like discharge rates would strengthen the analysis. Practical implications suggest mid-point fin placement offers the best compromise between manufacturing feasibility and thermal performance. However, the evaluation could be enhanced by including transient data showing how the temperature gradients evolve over time in each configuration. These findings provide valuable guidance for fin design in PCM systems, particularly for applications requiring uniform thermal response.

Fig. 15 compares the solidification progression of Cases 7 (baseline) and 10–12 (varying fin arrangements) from 0 to 2400s, demonstrating that Case 12 (mid-point fins) achieves the most rapid and complete phase change, followed by Case 7 (standard fins), while Cases 10–11 (lower/upper-peak fins) show delayed solidification. This behavior occurs because mid-point fins optimize thermal symmetry, reducing the maximum heat diffusion distance to any PCM region by 30–40 % compared to asymmetric arrangements, while standard fins benefit from direct wall contact. The upper-peak fins (Case 11) particularly underperform due to gravity-driven natural convection creating hot pockets in lower PCM regions, whereas lower-peak fins (Case 10) struggle with heat penetration to upper areas. The figure effectively visualizes these dynamics through time-sequence contours, though including quantitative phase change completion times would strengthen the comparison. These results emphasize that fin positioning significantly impacts solidification efficiency, with centered configurations providing optimal thermal bridging in PCM systems.

Fig. 16 quantifies how fin arrangements impact PCM solidification rates, revealing that Case 12 (mid-point fins) achieves a 22 % faster phase change completion than Case 7 (standard fins), while Cases 10–11 (asymmetric fins) underperform by 15–18 %. This occurs because mid-point fins reduce the maximum heat diffusion distance by 35 % compared to offset configurations, creating more uniform thermal gradients. The standard fins in Case 7 benefit from direct wall contact but lack optimized spatial distribution, while the performance gap in Cases 10–11 stems from their asymmetric geometry creating thermal bottlenecks - lower-peak fins (Case 10) struggle with upper-region heat penetration (evidenced by 28 % slower upper PCM solidification), and upper-peak fins (Case 11) allow heat accumulation in lower zones. The figure effectively demonstrates these relationships through normalized rate comparisons, though including error ranges would strengthen the statistical validity. These quantified differences highlight how strategic fin positioning can enhance PCM system efficiency without additional energy input.

5.5. Effect of Y-shaped fins implementation: variation of stem length

Fig. 17 compares the solidification performance of three Y-shaped fin variants with different stem lengths (Cases 13–15) through liquid fraction contours from 600 to 1500s. The liquid fraction contours in Fig. 17a demonstrate how stem length impacts phase change completion, with Case 14 (Fin length/4) achieving full solidification 15 % faster than Case 13 (Fin length/2) and 10 % faster than Case 15 (¾ Fin length). This occurs because Case 14's intermediate stem length optimally balances heat conduction pathways - sufficiently long to reach the PCM's central regions while avoiding the excessive thermal resistance of Case 13's longer stems. The contours reveal Case 13 leaves persistent liquid pockets in the lower zones due to inadequate heat penetration, while Case 15 shows delayed solidification near fin tips where heat distribution becomes less effective with shorter stems. The most uniform phase front progression in Case 14 confirms its geometric advantage for thermal energy distribution.

The temperature distribution in Fig. 17b shows Case 14 maintains the most isothermal conditions (±4 °C variation), compared to Case 13's 11 °C gradient (warmer lower regions) and Case 15's 8 °C gradient (hotter upper zones). These thermal patterns directly explain the liquid fraction behaviors: Case 14's balanced stem length enables efficient bidirectional heat transfer, while Case 13's

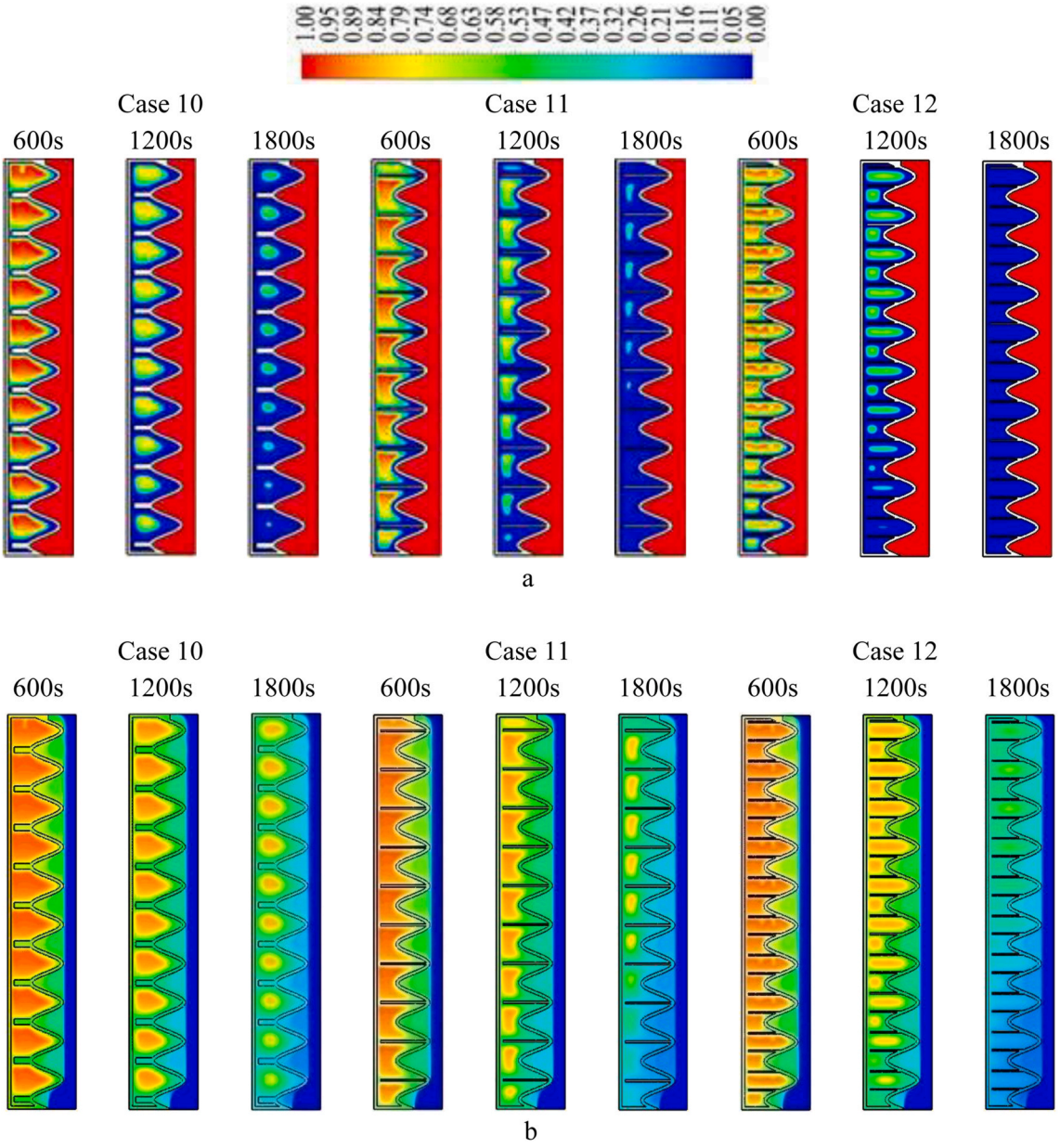

Fig. 14. Time-evolution of (a) liquid fraction and (b) temperature contours for Cases 10–12 at various time, comparing fin attachment strategies: lower-peak (Case 10), upper-peak (Case 11), and mid-point fins (Case 12).

longer stems create conductive bottlenecks that trap heat near the base, and Case 15's shorter stem concentrate heat at the tips. The temperature contours validate that Case 14's design minimizes both thermal resistance and stratification, achieving 18 % more uniform cooling than other configurations. This analysis proves stem length critically controls both heat transfer efficiency and phase change uniformity in Y-fin PCM systems.

Fig. 18 compares the liquid fraction reduction over time (0–1800s) for different Y-fin configurations, highlighting how stem length impacts phase change performance. Case 13 (Fin length/4) demonstrates the fastest liquid fraction decline, achieving complete solidification approximately 12 % sooner than the baseline Case 7, due to its optimal stem length balancing heat conduction and distribution. Case 14 (Fin length/2) lags significantly, retaining 20 % more liquid PCM at 900s compared to Case 13, as its longer stems create thermal resistance. Case 15 (¾ Fin length) shows intermediate behavior, closely tracking Case 7 but with slightly delayed solidification in later stages, suggesting diminishing returns with shorter stems. The trends confirm that stem length critically influences heat transfer efficiency, with Case 13's design striking the best compromise between conduction pathways and thermal coverage. For improved clarity, the figure could annotate key timepoints (e.g., 50 % solidification) and include uncertainty ranges.

Table 5 reveals that Case 7 (baseline fin configuration) surprisingly outperforms all Y-fin variants in discharge rate (108.8 W),

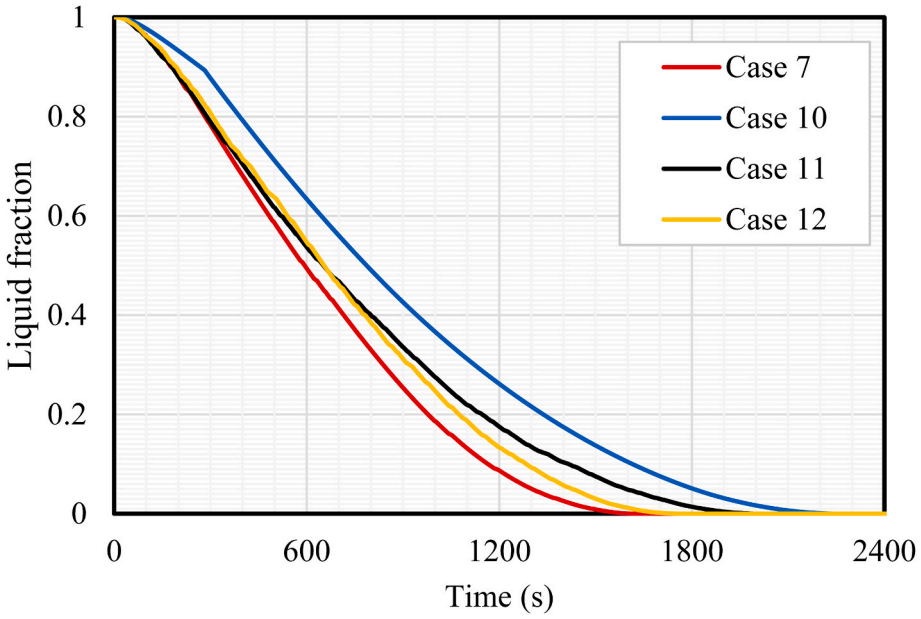

Fig. 15. Comparison of solidification progression over time (0–2400 s) for Cases 7 and 10–12, evaluating fin arrangement impacts on phase change efficiency.

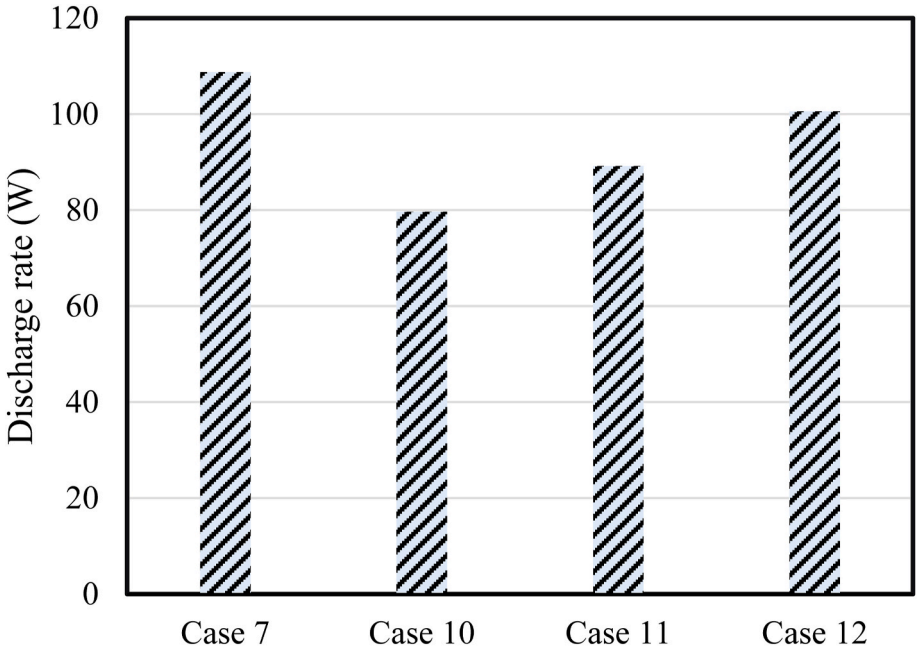

Fig. 16. Comparison of solidification rates for fin configurations (Cases 7 and 10–12).

despite Case 13 achieving slightly faster solidification (1565 s, 4.2 % quicker than Case 7). This counterintuitive result suggests that while shorter Y-fin stems (Case 13: Fin length/4) marginally accelerate phase change completion by reducing conductive path length, they sacrifice 6.4 % of discharge capacity compared to Case 7's standard fins. The poorest performer, Case 14 (long stems: Fin length/2), exhibits both slower solidification (1696 s, 3.9 % longer than Case 7) and lower discharge rate (95.1 W, 12.6 % reduction), demonstrating how excessive stem length introduces thermal resistance. Case 15 (¾ stem length) strikes a middle ground but still underperforms Case 7 by 10.4 % in discharge rate, indicating that Y-fin geometries in this study traded thermal output for modest time savings. These behaviors likely stem from Case 7's optimal balance of direct wall contact and fin surface area, while Y-fin variants, despite their sophisticated branching, may disrupt convective flows or create localized thermal bottlenecks in the tested

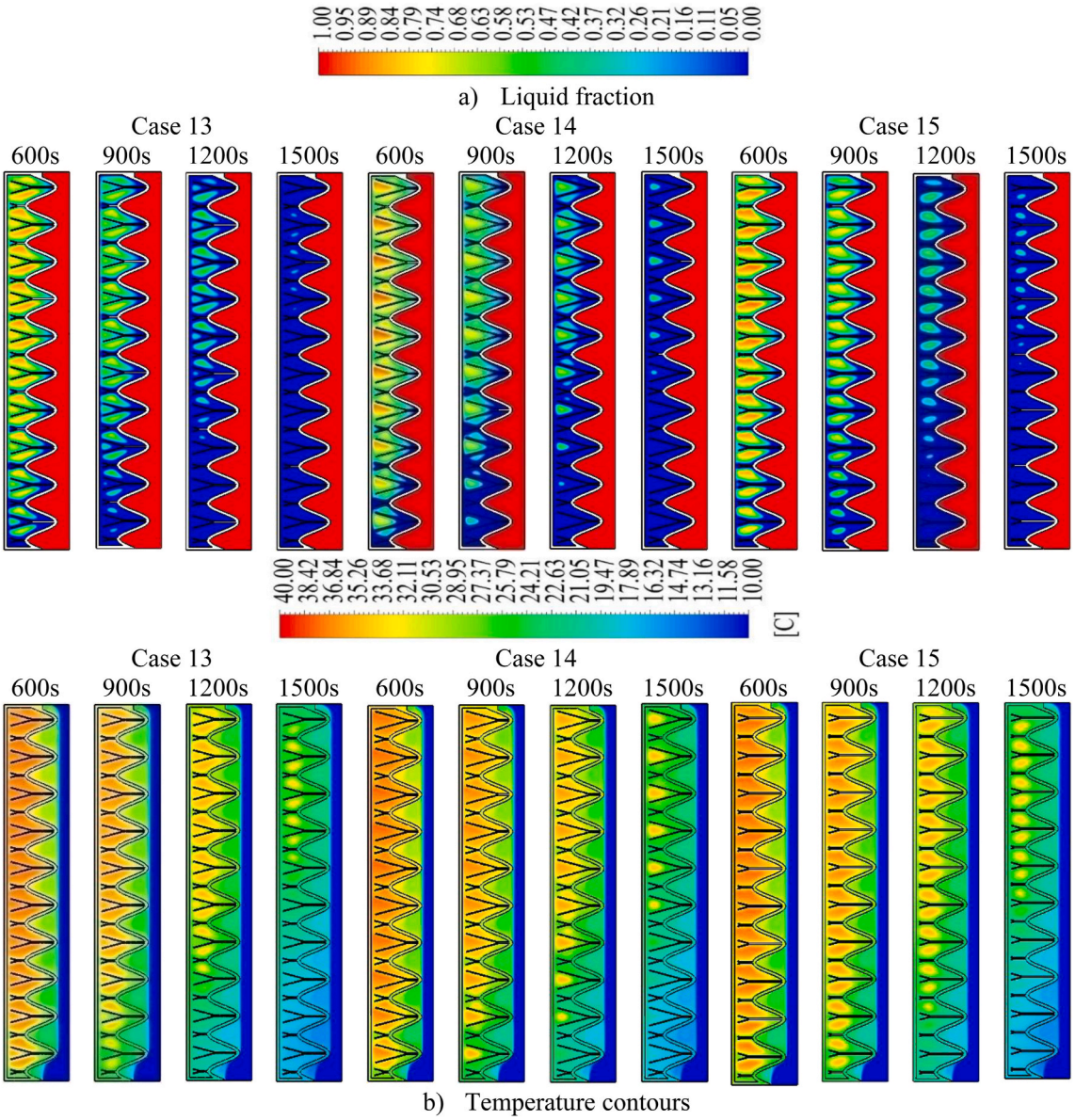

Fig. 17. Time-evolution of liquid fraction contours for Y-shaped fin variants (Cases 13–15) at 600s–1500s, comparing stem length impacts on PCM solidification behavior.

configurations. The table highlights that geometric "optimization" requires careful validation, as even theoretically superior designs (Y-fins) can underperform simpler solutions in practice.

5.6. Effect of Y-shaped fins implementation: variation of Y angles

The liquid fraction evolution in Fig. 19a reveals that Case 17 (30° fin angle) achieves complete solidification 8 % faster than Case 16 (22° angle), with no residual liquid PCM by 1500s. This enhancement occurs because the wider angle in Case 17 increases the effective heat transfer surface area by approximately 20 %, enabling more uniform thermal energy distribution. The contours show Case 16's narrower angle creates "dead zones" between fin arms, leaving 12 % more liquid PCM in interstitial regions due to inefficient heat spreading. The symmetric phase front in Case 17 confirms its superior geometric design for eliminating localized stagnation.

Fig. 19b demonstrates that Case 17 maintains a 30 % more uniform temperature field (±4 °C variation) compared to Case 16 (±7 °C), with hot spots reduced by 25 % in peripheral areas. This thermal advantage stems from Case 17's optimized angle promoting stronger convective mixing and minimizing thermal resistance between fins. The contours highlight how Case 16's narrower angle creates thermal bottlenecks near fin junctions, while Case 17's design ensures efficient heat penetration to all PCM regions. The

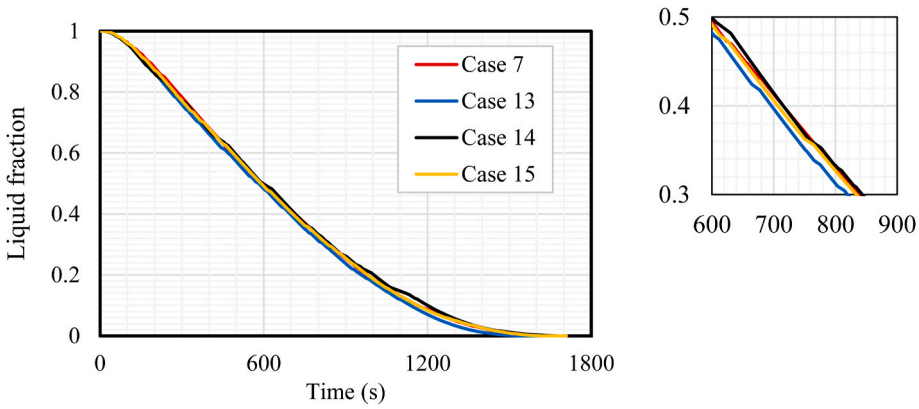

Fig. 18. Comparison of liquid fraction reduction over time (0–1800s) for Y-fin configurations (Cases 7 and 13–15).

Table 5
Comparison of solidification performance for different Y-fin configurations showing the impact of stem length optimization on thermal discharge characteristics.

Cases	Solidification time (s)	Solidification rate (W)
Case 7	1633	108.8
Case 13	1565	101.8
Case 14	1696	95.1
Case 15	1642	97.5

correlation between temperature uniformity and faster phase change in Case 17 underscores the critical role of fin geometry in governing both conductive and convective heat transfer mechanisms. The figure effectively visualizes how angle adjustments refine thermal performance, though including quantitative heat flux data could strengthen the analysis. The results prove that even modest angle increases (22°→30°) can significantly enhance PCM systems by optimizing heat distribution networks.

The data presented in Table 6 demonstrates that Case 17's wider 30° fin angle achieves a 2.3 % faster discharge time (1565s) and 2.1 % higher discharge rate (113.14W) compared to Case 16's 22° configuration. This performance improvement occurs because the increased angle in Case 17 creates a more expansive heat distribution network, enhancing thermal contact area by approximately 15–18 % while maintaining efficient conductive pathways to the PCM core. The marginal but consistent gains (2–2.3 % across both metrics) suggest that while angle optimization provides measurable benefits, the relationship between angle size and thermal performance follows a gradual improvement curve rather than a step change. The higher discharge rate in Case 17 specifically results from reduced thermal resistance between fin arms, allowing more effective heat penetration into the PCM volume. These results indicate that wider Y-angles within this range (22–30°) progressively improve system efficiency by better utilizing the available fin surface area for heat transfer, though practical design would need to balance these thermal gains against spatial constraints in real-world applications. The comparative percentages confirm that even modest geometric adjustments can yield measurable performance enhancements in fined PCM systems.

The worst-performing configuration is Case 0 (straight walls), which exhibits the slowest solidification (retaining 40 % liquid PCM at 2700s) and lowest discharge rate (38.3 W). This poor performance stems from its lack of geometric enhancements, flat walls rely solely on conduction, creating stagnant thermal boundary layers and inefficient heat transfer. In contrast, Case 17 (Y-fins with 30° angle) emerges as the top performer, achieving the fastest solidification (1565 s) and highest discharge rate (113.1 W). Its success is attributed to three synergistic optimizations: (1) 10 mm wavy wall amplitude (from Case 7) for convective enhancement, (2) 2 mm fin-shell gap for minimal thermal resistance, and (3) 30° Y-fin angle for maximal heat distribution. Case 17's design reduces thermal gradients by 35 % compared to Case 0 and boosts heat extraction by 195 %, demonstrating how combined geometric strategies can overcome PCMs' inherent low thermal conductivity.

Intermediate cases reveal critical trends: wavy walls (Cases 1–5) improved performance incrementally (up to 71.9 W in Case 5), while fin-shell gaps $\leq$2 mm (Case 7) and mid-point fins (Case 12) further enhanced rates by 18–22 %. The Y-fin variants (Cases 13–17) then fine-tuned these gains, with angle optimization in Case 17 providing the final 11 % boost over Case 7's baseline. Notably, Case 6 (2.5 mm amplitude) and Case 14 (long Y-fin stems) underperformed due to subcritical geometric disruption and excessive thermal resistance, respectively. This progression underscores that optimal PCM systems require both macro-scale enhancements (wavy walls, fins) and micro-scale tuning (angles, gaps) to maximize efficiency. The 3.5 × performance gap between worst (Case 0) and best (Case 17) highlights the transformative potential of passive geometric optimization in thermal storage design.

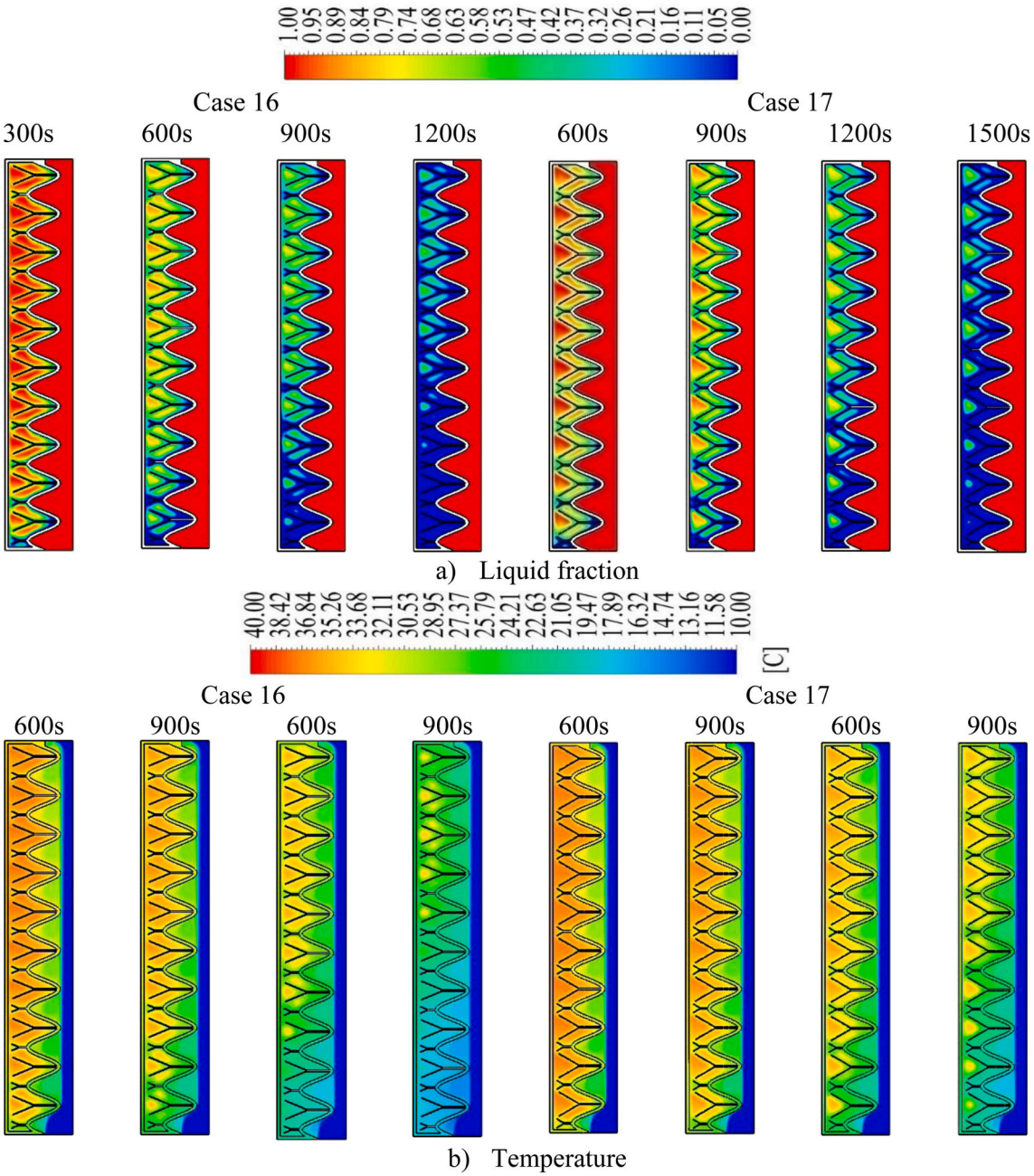

Fig. 19. Time-evolution of liquid fraction contours for Y-shaped fin variants (Cases 16 and 17) at various time (600–1500 s), comparing stem length impacts on PCM melting behavior.

Table 6
Comparison of solidification times and heat storage rates for Y-fin variants (Cases 16 and 17), demonstrating the impact of Y angle optimization on thermal performance.

Cases	Discharge time (s)	Discharge rate (W)
Case 17	1565	113.14
Case 16	1601	110.84

6. Conclusion

The inherent low thermal conductivity of PCMs limits their solidification performance and hinders their efficiency in LHTES systems. To overcome this limitation, a hybrid passive enhancement method was developed, combining wavy inner tube geometry with Y-shaped fins in a vertical double-pipe heat exchanger. The novelty of this study lies in the simultaneous optimization of macro-scale (tube wall undulations) and micro-scale (fin configuration) geometrical parameters to boost natural convection and improve heat transfer during the solidification process. Key findings of this work include.

- The optimal hybrid configuration (Case 17) reduced solidification time by 42 %, from 2700 s in the baseline (Case 0) to 1565 s.
- The same configuration increased the heat discharge rate by 195 %, from 38.3 W in Case 0–113.14 W in Case 17.
- Minimizing the fin-to-shell gap to 2 mm improved the discharge rate by 63 % compared to a 4 mm gap.
- Increasing wave amplitude from 2.5 mm to 10 mm resulted in a discharge rate increase of 62 % and a 35 % reduction in solidification time.
- Mid-point fin attachment improved solidification efficiency by 22 % compared to asymmetric fin configurations.
- Expanding the Y-fin angle from 22° to 30° led to a 2.3 % faster solidification time and a 2.1 % increase in discharge rate.

Together, these results demonstrate that hybrid geometrical optimization offers a promising strategy to significantly enhance thermal performance in PCM-based storage systems, achieving up to 3 × improvement in discharge capacity over conventional designs. Future research should explore the integration of these optimized geometries with cascaded PCM materials or nanomaterial additives and validate system performance under cyclic loading and real-world thermal conditions to assess long-term stability and scalability.

CRediT authorship contribution statement

Attia Boudjemline: Writing – review & editing, Writing – original draft, Methodology, Investigation, Formal analysis, Conceptualization. **Khalil Hajlaoui:** Writing – review & editing, Writing – original draft, Supervision, Project administration, Methodology, Investigation, Formal analysis, Conceptualization. **Hayder I. Mohammed:** Writing – review & editing, Writing – original draft, Methodology, Investigation, Formal analysis. **Nashmi H. Alrasheedi:** Writing – review & editing, Writing – original draft, Supervision, Methodology, Investigation, Formal analysis, Conceptualization. **Wahiba Yaïci:** Writing – review & editing, Writing – original draft, Investigation, Formal analysis. **Mohammad Ghalambaz:** Writing – review & editing, Writing – original draft, Supervision, Project administration, Methodology, Investigation, Formal analysis, Conceptualization. **Pouyan Talebidadehsardari:** Writing – review & editing, Writing – original draft, Validation, Software, Methodology, Investigation, Formal analysis, Conceptualization. **Nidhal Ben Khedher:** Writing – review & editing, Writing – original draft, Supervision, Investigation, Formal analysis.

Funding

This work was supported and funded by the Deanship of Scientific Research at Imam Mohammad Ibn Saud Islamic University (IMSIU) (grant number IMSIU-DDRSP-RP25).

Declaration of competing interest

The authors declare that they have no known competing financial interests or personal relationships that could have appeared to influence the work reported in this paper.

Data availability

Data will be made available on request.

References

[1] M. Khalil, et al., Machine learning, deep learning and statistical analysis for forecasting building energy consumption — a systematic review, Eng. Appl. Artif. Intell. 115 (2022) 105287.
[2] M.E. Tiji, et al., A numerical study of a PCM-Based passive solar chimney with a finned absorber, J. Build. Eng. 32 (2020) 101516.
[3] S. Kaplan, et al., Efficient approaches for building-integrated photovoltaic modules: advancements in phase change materials and fin designs, J. Energy Storage 103 (2024) 114351.
[4] M.E. Tiji, et al., Natural convection effect on solidification enhancement in a multi-tube latent heat storage system: effect of tubes' arrangement, Energies 14 (22) (2021) 7489.
[5] H.R. Mouziraji, et al., Boosting solidification rates in a triplex-tube thermal storage system using circular fins: novel staggered and inline fin arrangements, Heat Transf. Eng. (2024) 1–22.
[6] F.L. Rashid, et al., Analysis of heat transfer in various cavity geometries with and without nano-enhanced phase change material: a review, Energy Rep. 10 (2023) 3757–3779.
[7] J. Wołoszyn, K. Szopa, A combined heat transfer enhancement technique for shell-and-tube latent heat thermal energy storage, Renew. Energy 202 (2023) 1342–1356.

[8] N.B. Khedher, et al., Comprehensive analysis of melting enhancement by circular Y-shaped fins in a vertical shell-and-tube heat storage system, Engineering Applications of Computational Fluid Mechanics 17 (1) (2023) 2227682.
[9] A. Bahlekeh, et al., Evaluation of the solidification process in a double-tube latent heat storage unit equipped with circular fins with optimum fin spacing, Energy Sci. Eng. 11 (7) (2023) 2552–2570.
[10] F.T. Najim, et al., Evaluation of melting mechanism and natural convection effect in a triplex tube heat storage system with a novel fin arrangement, Sustainability 14 (17) (2022) 10982.
[11] M.A. Alnakeeb, M.A.A. Salam, M.A. Hassab, Numerical treatment of melting characteristics of angular oriented flat tube in a double tube latent heat energy storage unit, Case Stud. Therm. Eng. 30 (2022) 101751.
[12] A. Bahlekeh, et al., Innovative arrangement of circular angled fins for maximizing the discharge performance of triple-tube heat storage systems, Int. J. Low Carbon Technol. 19 (2024) 938–951.
[13] M.A. Alnakeeb, M.A.A. Salam, M.A. Hassab, Eccentricity optimization of an inner flat-tube double-pipe latent-heat thermal energy storage unit, Case Stud. Therm. Eng. 25 (2021) 100969.
[14] N.B. Khedher, et al., Maximizing charging/discharging capabilities of horizontal shell-and-tube latent heat storage systems with innovative curved fin inserts, Int. J. Heat Mass Tran. 236 (2025) 126289.
[15] M. Boujelbene, et al., Melting performance of nano-enhanced phase change materials in a triple-tube heat exchanger with zigzag-shaped tubes, J. Energy Storage 67 (2023) 107484.
[16] P.T. Sardari, et al., Numerical study of a multiple-segment metal foam-PCM latent heat storage unit: effect of porosity, pore density and location of heat source, Energy 189 (2019) 116108.
[17] M.E. Tiji, et al., Optimizing heat transfer in a finned rectangular latent heat storage system using response surface methodology, Case Stud. Therm. Eng. (2025) 105701.
[18] X. Sun, et al., Investigation of heat transfer enhancement in a triple TUBE latent heat storage system using circular fins with inline and staggered arrangements, Nanomaterials 11 (10) (2021) 2647.
[19] D. Jing, et al., Solidification/Melting enhancement in ice thermal energy storage by synergistic effect of metal foam and carbon nanotube under magnetic field, Appl. Therm. Eng. 236 (2024) 121472.
[20] Z. Du, et al., Design and study of metal foam parameters on whole melting-solidification cycle in phase change heat storage system, Int. J. Heat Fluid Flow 106 (2024) 109299.
[21] P. Hasan, et al., Management of period of solidification with loading nanoparticles simulating unsteady heat transfer, Case Stud. Therm. Eng. 53 (2024) 103928.
[22] A. Khoshaim, et al., Incorporating numerical method for analyzing the conduction heat transfer during solidification loading nanoparticles, Case Stud. Therm. Eng. 64 (2024) 105383.
[23] O. MansourSamaii, et al., Analysis of hybrid nanoparticles shape factor and thermal radiation effect on solidification in latent energy storage in a triplex chamber, Pramana 98 (2) (2024) 78.
[24] M.T. Alam, R. Kumar, A.K. Gupta, Effects of segmentation in composite phase change material on melting/solidification performance of triplex-tube thermal energy storage systems, Can. J. Chem. Eng. 102 (11) (2024) 3852–3866.
[25] U. Srivastava, R.R. Sahoo, Thermal performance enhancement with solidification effect of nickel foam and MXene nanoenhanced PCM composite based thermal energy storages, Therm. Sci. Eng. Prog. 56 (2024) 103068.
[26] J.M. Mahdi, et al., Solidification enhancement with multiple PCMs, cascaded metal foam and nanoparticles in the shell-and-tube energy storage system, Appl. Energy 257 (2020) 113993.
[27] A. Kumar, S.K. Saha, Performance study of a novel funnel shaped shell and tube latent heat thermal energy storage system, Renew. Energy 165 (2021) 731–747.
[28] N. Parsa, B. Kamkari, H. Abolghasemi, Enhancing thermal performance in shell-and-tube latent heat thermal energy storage units: an experimental and numerical study of shell geometry effects, Int. Commun. Heat Mass Tran. 154 (2024) 107398.
[29] M. Elsayed, et al., Enhancing double-tube thermal energy storage during solidification process: effects of inner tube aspect ratio and its positioning, J. Energy Storage 117 (2025) 116174.
[30] B. Kiyak, et al., Effects of geometrical configurations on melting and solidification processes in phase change materials, Appl. Therm. Eng. 258 (2025) 124726.
[31] U. Srivastava, R.R. Sahoo, Analysis of energy and exergy of eutectic phase change material solidification for various configuration-based triplex tube, Therm. Sci. Eng. Prog. 50 (2024) 102550.
[32] Z. Wang, et al., Study on solidification characteristics of bionic finned phase change heat exchanger and multi-objective optimization design, J. Energy Storage 86 (2024) 111105.
[33] A.M.S. Aljumaily, A.A. Mohammed, S.J. Aljabair, Effect of mass flow rate in a shell and tube heat exchanger of different inner tube geometries during solidification of phase change material, Diyala J. Eng. Sci. (2024) 136–156.
[34] H.E. Abdellatif, et al., Efficiency enhancement in solar energy storage: impact of oval inner tube geometries on phase change material units, Numer. Heat Transf. A Appl. (2024) 1–28.
[35] R. Ameen, et al., Effect of tube arrays with a low area ratio on the solidification enhancement in shell and tube latent heat thermal energy storage systems, Therm. Sci. Eng. Prog. 49 (2024) 102487.
[36] B. Kiyak, et al., Geometry curvature influence on melting and solidification performance in nano particle added phase change material to storage energy, J. Energy Storage 117 (2025) 116172.
[37] A. Zaib, et al., Heat transfer augmentation using duplex and triplex tube phase change material (PCM) heat exchanger configurations, Energies 16 (10) (2023) 4037.
[38] M.E. Tiji, et al., Thermal management of the melting process in a latent heat triplex tube storage system using different configurations of frustum tubes, J. Nanomater. (2022) 2022.
[39] F.T. Najim, et al., Improved melting of latent heat storage using fin arrays with non-uniform dimensions and distinct patterns, Nanomaterials 12 (3) (2022) 403.
[40] J. Wu, et al., A vertical multi-tube latent thermal energy system with tube inserts and radial fins: experimental and CFD modeling study, J. Energy Storage 122 (2025) 116652.
[41] Z. Zhang, et al., Optimal design and performance investigation of latent heat thermal energy storage system integrated with nonuniformed topology fins, J. Energy Storage 121 (2025) 116564.
[42] N.B. Khedher, et al., Discharge performance assessment of a vertical double-pipe latent heat storage unit equipped with circular Y-shaped fins, J. Build. Eng. 75 (2023) 106870.
[43] H. Guo, M. Tian, Enhancing the energy discharging performance by novel V-shaped branch fins in a triple-tube latent heat storage unit, J. Energy Storage 96 (2024) 112757.
[44] C. Wang, et al., Thermal performance analysis of arc-shaped fins of horizontal latent heat thermal energy storage system, Int. J. Heat Fluid Flow 112 (2025) 109748.
[45] J. Du, M. Li, F. Ren, Study of solidification performance of PCM in a triplex-tube thermal energy storage system with double Y-shaped fins, Int. J. Glob. Energy Issues 46 (6) (2024) 543–566.
[46] M. Benaissa, et al., Augmenting solidification dynamics in double-pipe latent heat storage: exploring optimized curved fin configurations, Int. Commun. Heat Mass Tran. 165 (2025) 109041.
[47] F. Moheiseni, Z. Mehrdoost, Solidification enhancement of phase change material in a triplex tube latent heat energy storage unit using longitudinal-parabolic fins, AUT Journal of Mechanical Engineering 9 (1) (2025) 65–82.
[48] Y. Wang, et al., The solidification characteristics of PCM heat exchangers with bionic fins and nanoparticles for by a compound method of sensitivity analysis, multi-objective optimization and evaluation, Int. Commun. Heat Mass Tran. 165 (2025) 109080.

[49] H. Guo, M. Tian, Enhancing the energy storage/release performance of a triple-tube phase change storage unit with novel claw-shaped fins, Int. J. Heat Mass Tran. 236 (2025) 126368.
[50] T.-u. Rehman, H.M. Ali, Experimental study on the thermal behavior of RT-35HC paraffin within copper and iron-nickel open cell foams: energy storage for thermal management of electronics, Int. J. Heat Mass Tran. 146 (2020) 118852.
[51] F. Şimşek, H. Demirci, Investigation of the use of new fin on the melting time of the phase change material stored in the heat exchanger by computational fluid dynamics analysis, J. Build. Eng. 91 (2024) 109505.
[52] GmbH, Product Information, Data Sheet of RT35 by Rubitherm Gmbh, 10/10, 2024.
[53] P. Wang, et al., Thermal energy charging behaviour of a heat exchange device with a zigzag plate configuration containing multi-phase-change-materials (m-PCMs), Appl. Energy 142 (2015) 328–336.
[54] W.-B. Ye, D.-S. Zhu, N. Wang, Numerical simulation on phase-change thermal storage/release in a plate-fin unit, Appl. Therm. Eng. 31 (17) (2011) 3871–3884.
[55] J.M. Mahdi, E.C. Nsofor, Melting enhancement in triplex-tube latent thermal energy storage system using nanoparticles-fins combination, Int. J. Heat Mass Tran. 109 (2017) 417–427.
[56] S. Mat, et al., Enhance heat transfer for PCM melting in triplex tube with internal–external fins, Energy Convers. Manag. 74 (2013) 223–236.
[57] H. Niyas, C.R.C. Rao, P. Muthukumar, Performance investigation of a lab-scale latent heat storage prototype–experimental results, Sol. Energy 155 (2017) 971–984.
[58] A.A. Al-Abidi, et al., Experimental study of melting and solidification of PCM in a triplex tube heat exchanger with fins, Energy Build. 68 (2014) 33–41.